A stress-response-related inter-compartmental signalling pathway regulates embryonic cuticle integrity in Arabidopsis

Audrey Creff[1], Lysiane Brocard[2], Jérôme Joubès[3,4], Ludivine Taconnat[5], Nicolas M. Doll[1], Stephanie Pascal[3,4], Roberta Galletti[1], Anne-Charlotte Marsollier[1], Steven Moussu[1], Thomas Widiez[1], Frédéric Domergue[3,4*], and Gwyneth Ingram[1*]

[1] Laboratoire Reproduction et Développement des Plantes, Univ Lyon, ENS de Lyon, UCB Lyon 1, CNRS, INRA, F-69342, Lyon, France.

[2] CNRS/ University of Bordeaux, Plant Imaging Platform of Bordeaux Imaging Center, UMS 3420, F-33000 Bordeaux, France

[3] Université de Bordeaux, Laboratoire de Biogenèse Membranaire, UMR5200, F-33000 Bordeaux, France.

[4] CNRS, Laboratoire de Biogenèse Membranaire, UMR5200, F-33000 Bordeaux, France.

[5] Institut of Plant Sciences Paris-Saclay (IPS2), UMR 9213/UMR1403, CNRS, INRA, Université Paris-Sud, Université d'Evry, Université Paris-Diderot, Sorbonne Paris-Cité, Bâtiment 630, 91405 0rsay, France

* Authors for correspondence (Gwyneth.Ingram@ens-lyon.fr; Frederic.Domergue@u-bordeaux.fr)

ABSTRACT

The embryonic cuticle is necessary for normal seed development and seedling establishment in Arabidopsis. Although mutants with defective embryonic cuticles have been identified, neither the deposition of cuticle material, nor its regulation, has been described during embryogenesis. Here we use electron microscopy, lipid staining and permeability assays to show that cuticle deposition initiates *de novo* in patches on globular embryos. By combining these techniques with genetics and gene expression analysis, we show that successful patch coalescence to form a continuous cuticle requires a signalling involving the endosperm-specific subtilisin protease ALE1 and the receptor kinases GSO1 and GSO2, which are expressed in the developing embryonic epidermis. Transcriptome analysis shows that this pathway regulates stress-related gene expression in seeds. Consistent with these findings we show genetically, and through activity analysis, that the stress-associated MPK6 protein acts downstream of GSO1 and GSO2 in the developing embryo. We propose that a stress-related signalling pathway has been hijacked in some angiosperm seeds through the recruitment of endosperm-specific components. Our work reveals the presence of an inter-compartmental dialogue between the endosperm and embryo that ensures the formation of an intact and functional cuticle around the developing embryo through an "auto-immune" type interaction.

INTRODUCTION

The Arabidopsis seed is a complex structure composed of three genetically distinct compartments, the maternally-derived seed coat, the embryo, and the endosperm. After fertilization the expansion of the endosperm drives the growth of the seed. However, during later developmental stages the

endosperm breaks down, leaving space for the growing embryo. By the end of seed development, only a single endosperm cell layer envelops the embryonic tissues (reviewed in [1]).

The endosperm is an angiosperm innovation, thought to have arisen through the sexualisation of the central cell of the female gametophyte [2]. The ancestors of angiosperms probably had seeds more similar to those of gymnosperms, in which tissues of the female gametophyte proliferate independently of egg cell fertilization to produce a nutrient rich storage tissue. However, the endosperm plays not only a nutritional role, but also a role in regulating embryo development. For example, the peptide CLAVATA3/EMBRYO SURROUNDING REGION-RELATED8 (CLE8) may act non-cell autonomously to regulate early Arabidopsis embryogenesis [3]. Recently, maternally-expressed peptides present in the central cell pre-fertilization, and subsequently in the early EMBRYO SURROUNDING REGION (ESR), were shown to regulate Arabidopsis suspensor development. Genetic analysis suggests that this regulation could be mediated by a pathway involving the Receptor-Like Cytoplasmic Kinase SHORT SUSPENSOR [4,5], although the receptor involved remains unidentified.

In previous works we showed genetically that the ESR-specific subtilisin protease Abnormal LEaf-shape1 (ALE1) acts in the same genetic pathway as two embryonically-expressed receptor kinases, GASSHO1 [(GSO1) also known as SCHENGEN3 [6]] and GASSHO2 (GSO2), to control the formation of the embryonic cuticle in developing seeds [7-10]. Our results indicate that a seed specific inter-tissue signalling event is necessary for the formation of a functional embryonic cuticle [7]. The results of genetic studies have led us to speculate that the role of this pathway is to ensure the robust elimination of apoplastic continuity between the developing embryo and the surrounding endosperm thus gating molecular movement between the two compartments [11,12].

71

72 The cuticle is the outermost layer of the aerial parts of the plant. It is a highly complex
73 structure mainly composed of a lipid polymer (cutin) and waxes, either associated with the
74 polymer (intracuticular waxes) or deposited on the top of it (epicuticular waxes) (recently
75 reviewed in [13,14]). Cutin and waxes are composed of complex mixtures of hydroxylated and
76 very long-chain fatty acid derivatives, respectively. Cuticle structure and composition are highly
77 regulated not only at the tissue level, but also in response to environmental stimuli such as
78 drought, radiation and pollution [13,14]. In addition, several reports have highlighted the
79 important role played by the cuticle in biotic interactions, and particularly in protecting plants
80 from attack by bacterial pathogens (reviewed in [13,15,16]).

81 In Arabidopsis although little, if any, evidence exists for the presence of cutin-like
82 substances in the wall between the mature egg cell and the central cell, by the end of
83 embryogenesis the hypocotyl and cotyledons of the embryo are covered with a continuous cuticle
84 which renders the germinating seedling impermeable to hydrophilic dyes, and resistant to water
85 loss [17]. Cuticle biogenesis is considered to be a unique property of epidermal cells [18]. During
86 plant development, epidermal cells are generated by anticlinal divisions of pre-existing epidermal
87 cells so that each cell inherits an intact external cuticularised cell wall. In this respect the
88 embryonic cuticle is atypical as it is deposited *de novo* at the interface between the developing
89 embryo and endosperm. Although mutants with defective embryonic cuticles have been described
90 [7-10,17], only very fragmentary evidence about when the embryonic cuticle appears is present in
91 the literature. Furthermore, the structure of the embryonic cuticle, its composition, the
92 mechanisms via which it is deposited and its function during seed development remain
93 unexplored. In this study we aimed to elucidate how the embryonic cuticle is formed, and to
94 investigate how the ALE1 GSO1 GSO2 signalling pathway impacts its biosynthesis and
95 deposition.

96

97 **RESULTS**

98 Expression of genes involved in cuticle deposition initiates during early embryogenesis.

99 An inspection of available *in silico* data [19-21] showed that many genes encoding enzymes
100 thought to be involved in cutin biosynthesis are expressed during early embryogenesis
101 (Supplementary Figure 1). *In situ* hybridisations confirmed that genes known to affect cuticle
102 production (*LACS2* [22,23], *FIDDLEHEAD/KCS10* [24-27], *LACERATA* [28] and
103 *BODYGUARD* [29]) or export (*LTPG1* [30] and *ABCG11* [31]) have a clear epidermis-
104 specific expression from the mid globular stage onwards (Figure 1, Supplementary Figure 2,
105 Supplementary Figure 3).

106 In agreement with published and *in silico* data [9] (Supplementary Figure 1) *GSO1*
107 and *GSO2* were expressed in the embryo from early developmental stages (Figure 1,
108 Supplementary Figure 3). In addition, their expression was mainly restricted to the embryonic
109 epidermis. *GSO1* expression in the embryonic epidermis was further confirmed using plants
110 expressing a functional genomic GSO1-mVENUS fusion under the control of the *GSO1*
111 promoter (*pGSO1*:*GSO1-mVENUS*) [6] (Figure 2). This construction fully complemented the
112 cuticle permeability phenotype of *gso1-1 gso2-1* double mutant seedlings, and strongly
113 reduced the misshapen-seed phenotype of *gso1-1 gso2-1* mutant seeds when introduced into
114 the *gso1-1 gso2-1* mutant background (Figure 2).

115 Since previous results showed that epidermal identity is not affected in *gso1-1 gso2-1*
116 mutants [12], the expression of cuticle biosynthesis genes was analysed by *in situ*
117 hybridization in *gso1-1 gso2-1* double mutant seeds (which show a stronger cuticle phenotype
118 than *ale1-4* mutants [7]). As shown in Figure 1 (and Supplementary Figure 2, Supplementary
119 Figure 3), no reduction in the expression of any of the cuticle biogenesis genes analysed was

120 detected in the embryonic epidermis of this background, whereas reduced expression of both
121 *GSO1* and *GSO2* was clearly visible. For these results, we concluded that although many
122 genes involved in cuticle biosynthesis are co-expressed with GSO1 and GSO2 in the
123 embryonic epidermis, their expression is not dependent upon GSO1 and GSO2.

124 Loss of GSO1/GSO2 and ALE1 function affects cuticle integrity

125 The cutin content of seedling cotyledons was assessed by measuring the quantities of the main
126 cutin monomers released after cutin isolation followed by depolymerisation (mainly C16 and
127 C18 ωOH (omega-hydroxy acid) and DCA (α,ω-dicarboxylic acid)). As clearly illustrated by
128 the quantification of 18:2-DCA, the major component of Arabidopsis cutin, a slight loss in
129 cutin load was detected in *gso1-1 gso2-1*, but not in *ale1-4* cotyledons compared to wild-type.
130 In contrast a very clear reduction in cutin load was observed in control plants lacking the
131 acyltransferases GPAT4 and GPAT8 required for cutin biosynthesis, as has previously been
132 reported in rosette leaves [32] (Figure 3a). We therefore investigated the cuticle permeability
133 of etiolated cotyledons by submerging them in the hydrophilic dye toluidine blue, which can
134 only penetrate internal tissues through defects in the cuticle [17]. Surprisingly, we found that
135 the cotyledons of etiolated *gpat4 gpat8* seedlings showed a rather similar toluidine blue
136 permeability to *ale1-4* seedlings and a considerably reduced permeability compared to *gso1-1*
137 *gso1-2* double mutants, suggesting that the *gpat4 gpat8* cuticle, although quantitatively
138 strongly deficient in cutin monomers, remains partially functional (Figure 3b). Taken together
139 with gene expression analysis, these results suggest that the ALE1, GSO1 and GSO2-
140 mediated signalling pathway might impact cuticle organisation or integrity rather than the
141 quantity of cuticle components produced by epidermal cells.

142 The process of embryonic cuticle deposition was investigated in more detail in wild-
143 type (Col-0) seeds (Figure 4a-d). At the two-cell stage the embryo was surrounded by a thick

144 cell wall but no electron dense material was detected at the embryo surface. At the mid-late
145 globular stage, a cutin-like electron-dense material was detected in patches (Figure 4b and
146 Supplementary Figure 5a,b). From heart stage onwards, an apparently continuous layer of
147 electron-dense cutin-like material was detected at the surface of the outer epidermal cell wall.
148 Embryonic cuticle production therefore involves the *de novo* deposition and subsequent
149 coalescence of "patches" of cuticular material at the surface of epidermal cells. Toluidine blue
150 assays with wild-type embryos extruded at different developmental stages indicated that
151 permeability started to reduce noticeably at the early torpedo stage (slightly after apparent gap
152 closure), and that the embryo continued to become more and more impermeable during
153 embryo development (Supplementary Figure 4), suggesting that the coalescence of gaps in the
154 embryonic cuticle correlates well with a reduction in embryonic permeability.

155 In *gso1-1 gso2-1* mutants the cuticle still showed discontinuities at the heart and
156 walking stick stage (Figure 4e-f, Supplementary Figure 5c-f). In this background the cuticle
157 also appeared thicker, but less condensed than that of wild-type embryos. The outer epidermal
158 cell wall was also abnormally thick at later stages (compare embryonic cell wall thickness in
159 Figure 4d with that in 4f). Similar discontinuities were observed, although at a lower
160 frequency, in the *ale1-4* background at the heart stage as described previously [10], but were
161 less frequent at later stages, consistent with the less severe cuticle permeability phenotype
162 observed in the seedlings of this background (Figure 4g-h). These results are consistent with
163 our hypothesis that the ALE1 GSO1 GSO2 pathway is necessary for generating a continuous
164 cuticle layer and further suggest that it controls "gap closure" during embryonic cuticle
165 maturation.

166 <u>GSO1 GSO2 and ALE1 regulate overlapping gene sets and promote the expression of defence</u>
167 <u>related genes during seed development.</u>

168 Transcriptional analysis of intact siliques from *gso1-1 gso2-1* and *ale1-4* mutants and wild-
169 type plants was carried out at globular and heart stages. The results are provided in Figure 5a
170 and b, Supplementary Table 1, and Supplementary Figures 6 and 7. The number of
171 differentially down-regulated genes in the mutant backgrounds compared to wild-type was
172 higher than the number of up-regulated genes (Supplementary Table 1). A moderate overlap
173 between genes showing higher expression in *ale1-4* and *gso1-1 gso2-1* mutants than wild-type
174 controls was observed (Supplementary Figure 6, Supplementary Table 1). In contrast more
175 than three quarters of the genes showing reduced expression at both developmental stages in
176 the *gso1-1 gso2-1* background also showed reduced expression at both developmental stages
177 in *ale1-4* mutants (Figure 5a and Supplementary Table 1), corroborating previously published
178 genetic evidence that ALE1, GSO1 and GSO2 act in the same genetic pathway [7]. Because
179 *ALE1* appears to be expressed exclusively in the ESR region of the endosperm [7,8,10], genes
180 mis-regulated in both mutant backgrounds likely comprise *bona fide* targets (direct and
181 indirect) of the ALE1 GSO1 GSO2 pathway, despite the fact that the expression of *GSO1* and
182 *GSO2* is not restricted to the seed [6,9,20].

183 Genes up-regulated in both mutant backgrounds showed a moderate over-
184 representation in GO terms associated with responses to abiotic stress (Supplementary Figure
185 6). In contrast, genes down-regulated in both backgrounds, particularly at the heart stage,
186 showed a very striking overrepresentation for GO terms linked to abiotic and biotic stress
187 responses (Figure 5b, Supplementary Figure 7). Mis-regulation of 19 of these genes was
188 validated using additional independent biological samples by qRT-PCR (Supplementary
189 Figure 8). The expression levels of these genes in seeds were generally low, and attempts to
190 carry out *in situ* hybridization were inconclusive. However for one target, *SWI3A* [33],
191 expression in the developing embryo predicted from *in silico* data was confirmed, and shown
192 to be convincingly reduced in embryos of the *gso1-1 gso2-1* double mutant (Supplementary

193 Figure 9). Thus, consistent with the embryonic expression of *GSO1* and *GSO2*, some of the
194 transcriptional regulation downstream of ALE1 GSO1 GSO2 signalling occurs in the embryo.
195 Expression of *ALE1* was not reduced in *gso1-1 gso2-1* mutants (Supplementary Table 2 and
196 Supplementary Figure 8), suggesting that ALE1 is not a downstream target of GSO1 GSO2-
197 mediated signalling, and could therefore act upstream of GSO1 and GSO2 in mediating
198 embryonic responses necessary for the establishment of an intact embryonic cuticle.

199 MPK6 acts in the ALE1 GSO1 GSO2 signalling pathway.

200 The GSO1 and GSO2 receptor kinases belong to family XI of the Leucine-Rich Repeat
201 (LRR)-RLKs [34,35], and are closely related to the "danger" peptide receptors PEPR1 and
202 PEPR2 [36,37], which are involved in the amplification of defence responses triggered by
203 pathogen-associated molecular pattern (PAMP) perception [38]. A previous study [39],
204 reported aberrantly shaped seeds, resembling those of *ale1-4* mutants, in Arabidopsis *mpk6*
205 mutants lacking the MITOGEN ACTIVATED PROTEIN KINASE6 (MPK6) protein, which
206 acts downstream of PEPR signalling. In addition a proportion of *mpk6* mutant seeds were
207 reported to rupture [39]. We confirmed these phenotypes in the *mpk6-2* mutant background
208 (Supplementary Figure 10). A recent article has suggested that some seed defects in *mpk6*
209 mutants may depend upon the genotype of the maternal tissues in the seed [40]. Reciprocal
210 crosses were therefore performed, and these confirmed that seed twisting phenotype is
211 dependent upon the genotype of the zygotic compartment and not the maternal compartment
212 (Supplementary Figure 11). We found that a proportion of *mpk6-2* seedlings showed
213 abnormal permeability to the hydrophilic dye toluidine blue, consistent with the presence of
214 cuticle defects (Figure 6). Nile red staining [32] of the cotyledons of etiolated seedlings was
215 used to confirm *mpk6* cuticle defects (Supplementary Figure 12 a,b). Using this technique,
216 wild-type cotyledons were found to be covered with a continuous lipid cuticle layer. As
217 previously reported, and consistent with our cutin analysis, *gpat4 gpat8* mutants showed

218 drastically reduced cuticle staining. In contrast *gso1-1 gso2-1* mutants showed a patchy
219 cuticle, similar to that seen using transmission electron microscopy on the embryo surface.
220 Both *ale1-4* and *mpk6-2* mutants showed a less well-defined cuticle than wild-type, which
221 although apparently continuous, showed uneven cutin deposition (Supplementary Figure 12
222 a,b).

223 Triple *mpk6-2 gso1-1 gso2-1* and double *ale1-4 mpk6-2* mutants were generated to
224 investigate further the genetic interactions of *ALE1, GSO1* and *GSO2* with *MPK6.* Fertility in
225 *ale1-4 mpk6-2* double mutants was similar to that in *mpk6-2* mutants, while triple *mpk6-2*
226 *gso1-1 gso2-1* mutant plants were viable but produced very few seeds. In terms of seed shape
227 and cotyledon cuticle permeability, triple *mpk6-2 gso1-1 gso2-1* mutants had phenotypes
228 identical to those observed in *gso1-1 gso2-1* double mutants (Figure 6, Supplementary Figure
229 10). Since all *gso1-1 gso2-1* mutant seeds are twisted, non-additivity cannot be concluded
230 from this phenotype. However, recent work has shown that additivity of toluidine blue
231 staining phenotypes can be detected in mutant combinations with *gso1-1 gso2-1 [41].* The
232 frequency of "twisted" seeds (including ruptured seeds), and toluidine blue stained seedling
233 cotyledons was non-additive in *ale1-4 mpk6-2* double mutant plants, consistent with *ALE1,*
234 *GSO1, GSO2* and *MPK6* acting in the same genetic pathway to control seedling cotyledon
235 permeability (Figure 6 and Supplementary Figure 10).

236 MPK6 is involved in a plethora of reproductive and non-reproductive developmental
237 processes and shows functional redundancy with other MPK proteins [39,42-52] meaning that
238 global transcriptome analysis in the *mpk6-2* background would likely be uninformative for
239 this study. We therefore directly tested a subset of genes mis-regulated in *gso1-1 gso2-1* and
240 *ale1-4* mutants for misregulation in *mpk6-2* mutants at three stages of embryo development.
241 Five out of eight genes tested showed reduced expression in *mpk6-2* either at all three stages
242 (*SWI3A, WRKY70* and *NIMIN1*), or in two out of three developmental stages tested (*SIB1* and

243 *NIMIN2*) (Supplementary Figure 13). Unsurprisingly given the relatively weak cuticle
244 phenotype of *mpk6* mutants compared with *gso1 gso2* mutants, some genes showing strong
245 down-regulation in the *gso1-1 gso2-1* mutants (*WRKY33, WRKY46 and WRKY53)* did not
246 show any significant reduction in expression in the *mpk6-2* mutant background
247 (Supplementary Figure 13) indicating that their transcriptional regulation downstream of
248 GSO1 and GSO2-mediated signalling could be dependent on signalling components acting
249 redundantly with MPK6. The expression of *ALE1, GSO1* and *GSO2* was not altered in *mpk6-*
250 *2* mutants (Supplementary Figure 13), indicating that MPK6 most probably acts downstream
251 of GSO1 and GSO2-mediated signalling.

252 To further confirm this hypothesis, we analysed MPK phosphorylation in developing
253 seeds from Col-0 and *gso1-1 gso2-1* double mutants. In seedlings, phosphorylation of MPK6
254 (and additional MPKs) can only be detected after elicitation (for example with the flg22
255 peptide). The response to flg22 is not attenuated in *gso1/gso2* mutant seedlings
256 (Supplementary Figure 14 and 15). In contrast, MPK6 phosphorylation (but not
257 phosphorylation of other MPKs) could be detected in un-elicited seeds (Figure 6b,
258 Supplementary Figure 16). Following quantification, we found that the degree of
259 phosphorylation of MPK6 was reduced by approximately 50% in *gso1-1 gso2-1* double
260 mutant seeds compared to wild-type, suggesting that a significant proportion of MPK6
261 phosphorylation in seeds depends on the activity of GSO1 and GSO2 (Figure 6c,
262 Supplementary Figure 16). Intriguingly, in seeds, a band corresponding to a second
263 phosphorylated MPK was detected exclusively in *mpk6-2* mutants (Figure 6b), suggesting that
264 the relatively weak *mpk6* seedling cuticle phenotype could be due to compensation by an as
265 yet unidentified MPK [53].

266 <u>MPK6 activity is required in the embryo, but not the endosperm, to maintain cuticle integrity.</u>

267 The strong expression of GSO1 and GSO2 in the embryonic epidermis, suggests that
268 the activity of GSO1 and GSO2 in cuticle formation is required in the embryo. No promoters
269 confirmed as specifically being expressed only in the embryo or embryo epidermis, have been
270 published. To further confirm the spatial requirement for GSO1/GSO2-dependent signalling
271 in the seed, we therefore complemented the *mpk6-2* mutant either with the *MPK6* cDNA
272 expressed under the ubiquitously expressed *RPS5A* promoter, or under the endosperm specific
273 *RGP3* promoter [54,55]. We were unable to complement either the misshapen seed/seed
274 bursting phenotypes or the toluidine blue permeability phenotypes of *mpk6-2* mutants by
275 expressing *MPK6* in the endosperm, but obtained full complementation of all phenotypes in
276 plants expressing *MPK6* under the *RPS5A* promoter (Figure 7, Supplementary Figures 17).
277 Together with the results of our reciprocal crosses, these findings indicate that the seedling
278 permeability phenotype of *mpk6-2* mutants is most likely due to signalling defects in the
279 embryo. Seed size and seed bursting defects could be caused by lack of MPK6 in the testa, as
280 suggested by reciprocal crosses, although this remains to be investigated in more detail. In
281 order to further confirm the function of MPK6 downstream of GSO1/GSO2 signalling we
282 attempted to express a constitutively active form of MPK6 under the *RPS5A* promoter in wild
283 type and double mutant plants, but were unable to generate any transformants, potentially due
284 to the critical roles played by MPK6 during early embryogenesis.

285 **DISCUSSION**

286 It this study, consistent with the similarity between GSO1/2 and PEPR1/2 proteins, we found
287 that stress-associated kinase MPK6, which has been shown to act downstream of PEPR
288 signalling [56], shows constitutive phosphorylation in developing seeds, and that this
289 phosphorylation is partially dependent upon GSO1 and GSO2. In addition, we showed that
290 GSO1/GSO2, are required for the expression of a set of stress-related genes during early seed
291 development. Our results suggest that GSO1/GSO2 dependent stress response-related

292 signalling pathways are active in developing seeds. Because of the conserved transcriptional
293 targets expressed downstream of GSO1/GSO2 dependent signalling, and in defence
294 responses, this scenario is distinct from previously reported situations in which single
295 pathway components, such as the co-receptor BAK1, play distinct roles in developmental and
296 defence-related signalling cascades through interaction with multiple receptors [57,58].
297 However, the role of the transcriptional targets of GSO1/GSO2 signalling in seeds remains to
298 be elucidated.

299 Our work also shows that GSO1/GSO2, ALE1 and MPK6 act in a genetic pathway
300 involved in ensuring embryonic cuticle integrity. We show for the first time that embryonic
301 cuticle biogenesis involves the coalescence of discontinuous patches of cutin-like material
302 that appear on the embryo surface at the globular stage, and that pathway mutants are either
303 incapable of completing, or retarded in the completion of "gap closure" during this process.
304 Interestingly, GSO1 (also known as SCHENGEN3 [6]) was recently shown to be involved in
305 ensuring the continuity of another apoplastic diffusion barrier, the Casparian strip, which
306 prevents the apoplastic movement of solutes from the cortex to the stele of the root [6]. GSO1
307 may therefore form part of a general mechanism employed by plants for monitoring the
308 "integrity" of apoplastic barriers formed during plant development.

309 The role of GSO1 and GSO2 in the closure of gaps in the nascent cuticle implies
310 spatial regulation of signalling outputs at the subcellular level. Cytoplasmic signalling
311 components which, like MPK6 might not be uncovered by transcriptome analysis but rather
312 are modified post-translationally, are therefore likely to be of critical importance in GSO1
313 GSO2 signalling in the embryonic epidermis. Indeed, although MPK6-mediated signalling
314 has most often been implicated in the control of transcription, particularly via the modulation
315 of the activity of WRKY transcription factors, evidence for potential roles in cytoplasmic

316 responses, for example during funicular guidance of pollen tubes [46] and control of cell
317 division planes [50], exist in the literature.

318 Cytoplasmic responses downstream of receptor-like kinases include the local
319 production of apoplastic Reactive Oxygen Species (ROS) and/or calcium influxes, and indeed
320 localized ROS production has been implicated in Casparian strip formation [6,59-61].
321 However although a plausible model has proposed that ROS release could mediate Casparian
322 strip polymerisation though polymerisation of monolignols [59], it is less obvious how ROS
323 could directly affect the biosynthesis of an aliphatic cutin-based barrier, although a possible
324 role for ROS in linking the cuticle to the cell wall has been evoked [62]. ROS production has
325 been shown to directly modulate the activation of MAPK signalling, providing a mechanism
326 permitting the reinforcement of localised signalling events [63,64]. Another, potentially
327 linked, possibility is that GSO1/GSO2 activity in the embryo could spatially direct the
328 secretion of either cuticle components or enzymes and cell wall components necessary for
329 their integration into the cutin polymer, in a system analogous to the rapid and highly
330 localized deposition of callose observed upon hyphal penetration into epidermal cells
331 (reviewed in [65,66]). Interestingly MPK6 has also been shown to be involved in
332 phragmoplast formation during root cell division and therefore could be involved in the
333 localised production/secretion of apoplastic compounds [50]. However, observing these
334 processes *in situ,* within the living seeds, would require developments in microscopy which
335 are not yet available.

336 Our work highlights several questions which merit further discussion. A first
337 important question is whether the GSO1/GSO2 signalling pathway could play a role in
338 protecting seeds, or more generally plants, against pathogen attack. Cuticle integrity in adult
339 plants has been shown to be required for resistance to *Pseudomonas* pathovars [67,68]. The
340 action of the ALE1 GSO1/GSO2 signalling pathway in ensuring embryonic cuticle integrity is

341 therefore likely to have a significant influence on embryo and seedling susceptibility to
342 bacterial pathogens. However, we have also shown that GSO1/GSO2, ALE1 and MPK6 are
343 necessary for the expression of known defence marker genes in seeds. Cuticle permeability
344 phenotypes have neither been reported in the literature for mutants affected in the defence
345 markers identified in our transcriptome studies, nor found in our own studies (unpublished
346 results). This raises the question of whether the ALE1, GSO1/GSO2, MPK6 signalling
347 pathway, in addition to mediating localised apoplastic modifications, could act at a more
348 global level either to protect developing seeds from the ingress of bacterial pathogens (thus
349 affecting vertical pathogen transmission), or to "prime" embryos against pathogen attack upon
350 germination. Exploring this possibility would necessitate functionally separating
351 susceptibility caused by cuticle defects from lack of immune priming, and will be technically
352 very challenging, but could ultimately inform strategies aiming to reduce vertical transmission
353 of plant pathogens.

354 The second question concerns how signalling via GSO1 and GSO2 is triggered in the
355 seed in the absence of pathogens. In this study we consolidate data supporting the function of
356 ALE1 in the same pathway as GSO1 and GSO2. We previously proposed that the function of
357 ALE1, GSO1 and GSO2 in ensuring the apoplastic separation of the embryo and endosperm
358 became necessary in angiosperms due to developmental constraints imposed by the
359 sexualisation of the female gametophyte, which led to the simultaneous development of the
360 embryo and surrounding nutritive tissues post-fertilization, rather than their sequential
361 development [11,12]. *ALE1* expression is endosperm specific and, as previously suggested
362 [69], the recruitment of *ALE1* to a function in reinforcing the embryonic cuticle may have
363 occurred during the emergence of the angiosperm lineage. Subtilases have been shown to be
364 involved in defence responses and immune priming in plants [70,71]. It is thus possible that
365 ALE1 acts to produce an as yet unidentified ligand for the GSO1 and GSO2 receptors. In such

366 a scenario the function of ALE1 in the seed could be analogous to the "immune priming"
367 function previously reported for the subtilase SBT3.3 [71].

368 Such a scenario naturally raises a third, and important question, around the identity of
369 the ligand of GSO1 and GSO2. Two sulfated peptides, CIF1 and CIF2, which can act as
370 ligands for GSO1 during Casparian strip formation, have recently been identified [72,73].
371 Testing the role of these molecules in developing seeds will be an obvious priority. However
372 Nakayama and colleagues specifically reported that no cuticle defects (as gauged by
373 cotyledon fusion phenotypes) were observed in *cif1 cif2* double mutants and the possibility
374 that other signalling molecules could be involved in ensuring embryonic cuticle integrity
375 therefore cannot be excluded.

376 In summary, we propose that endosperm-localised factors (like ALE1) may have been
377 recruited to hijack a defence-signalling pathway involving the ancestor(s) of GSO1 and
378 GSO2, and downstream signalling components including MPK6, and trigger an "auto-
379 immune" type response in the embryo to ensure cuticle integrity. The future identification of
380 further pathway components, and in particular the substrates of ALE1 and ligands of GSO1
381 and GSO2, will help to confirm this hypothesis.

382

383 **Materials and Methods**

384 **Plant material.** The *pGSO1*:GSO1-mVENUS line was kindly donated by Professor Niko
385 Geldner (Unil-Sorge, University of Lausanne). The *mpk6-2* (SALK_073907) mutant and the
386 *mpk3-1* (SALK-151594) were kindly provided by Dr Roberta Galletti.

387 **Growth conditions and plant treatments.** Unless otherwise specified, plants were grown for
388 10 d in sterile conditions on Murashige and Skoog (MS) agar plates with 0.5% sucrose, 1
389 month under short-day conditions (19°C, 8h light / 17°C, 16h dark) and then transferred to

390 standard long-day conditions (21°C, 16h light/8h dark) for one more month. To stage
391 material, newly opened flowers were marked each day for two weeks. For bacterial growth
392 assays, plants were grown under controlled conditions in a growth chamber at 21°C, with a 9-
393 hours light period and a light intensity of 190 $\mu mol.m^{-2}.s^{-1}$. For MPK6 activation analysis,
394 seedlings were grown for 10 d in MS liquid medium supplemented with 0.5% sucrose in
395 100µm cell strainers submerged in 6-well plates (5ml of medium per well). Cell strainers
396 were transferred to new plates containing MS sucrose 0.5% supplemented with 100 nM or 1
397 nM flg22 or water and incubated for 15 and 60 minutes at room temperature without skaking.
398 Seedlings were then rapidly harvested in liquid nitrogen and stored at -80 °C until protein
399 extraction. For cutin analysis of seedlings, seeds were sterilized, plated on MS medium
400 supplemented with 0.7 % agar, 0.7 % sucrose and 2.5 mM MES-KOH, pH 5.7, and stratified
401 in the dark for 3 days at $4^{o}C$. Plates were then transferred to a controlled environment growth
402 chamber at 22°C and with continuous light, and seedlings were grown for 5 days before
403 harvesting the cotyledons. For toluidine blue staining and Nile-Red staining, sterilized seeds
404 were spread uniformly on 15 cm MS plates with 0.5% sucrose and 0.4% Phytagel (Sigma)
405 (pH 5.8) and stratified for 2 days in the dark at 4°C. After stratification seeds were transferred
406 to a growth chamber and incubated for 6h under continuous light followed by 4 days in the
407 dark.

408 ***In situ* hybridization.** DNA templates for the probes used in *in situ* hybridizations were
409 amplified using the primers listed in Supplementary Table 2. Digoxigenin-labelled RNA
410 probes were produced and hybridized to tissue sections following standard procedures. In
411 brief, siliques were opened, fixed overnight in ice-cold PBS containing 4% paraformaldehyde,
412 dehydrated through an ethanol series, embedded in Paraplast Plus (Mc Cormick Scientific)
413 and sectioned (8 µm). Immobilized sections were dewaxed and hydrated, treated with 2x
414 saline sodium citrate (20 min), digested for 15 min at 37°C with proteinase K (20 mg/ml) in

415 50mM Tris-HCl, pH 7.5, 5mM EDTA), treated for 2 min with 0.2% glycine in PBS, rinsed,
416 postfixed with 4% paraformaldehyde in PBS (10 min, 4°C), rinsed, treated with 0.25% w/v
417 acetic anhydride in 100mM triethanolamine (pH 8.0 with HCl) for 10 min, rinsed and
418 dehydrated. Sections were then hybridized under coverslips overnight at 50°C with RNA
419 probes (produced using DIG RNA labelling kit (Roche)) diluted in DIG easy Hyb solution
420 (Roche) following the manufacturer's instructions. Following hybridization, the slides were
421 extensively washed in 0.1x saline sodium citrate and 0.5% SDS at 50 °C (3 h), blocked for 1
422 hour in 1% blocking solution (Roche) in TBS and for 30 minutes in BSA solution (1% BSA,
423 0.3% Triton-X-100, 100mM Tris-HCl, 100mM NaCl, 50mM $MgCl_2$), and then incubated in a
424 1/3000 dilution of in alkaline phosphatase-conjugated antidigoxigenin antibody (Roche) in
425 BSA solution for 2 h at RT. Sections were extensively washed in BSA solution, rinsed and
426 treated overnight in the dark with a buffered NBT/BCIP solution. Samples were rinsed in
427 water before air drying and mounting in Entellan (Sigma).
428
429 **Microscopy.** Embryos were imaged by gently bursting seeds between slide and cover-slip in
430 water and imaging using a dipping lens with a long working distance. Confocal imaging was
431 carried out on a Zeiss LSM700 with a W N-Acroplan 40x/0.75 M27 objective. mVENUS was
432 excited using a 488nm diode laser and fluorescence was collected using a 490-555 nm PMT.
433 Light microscopy imaging was carried out using a Zeiss axioimager 2. Images were acquired
434 using bright field illumination.

435 **Histochemical staining with Nile-Red.**

436 5-day-old etiolated seedlings were stained with Nile-Red (Sigma-Aldrich, stock solution at
437 1mg/mL in DMSO) at 2µg/mL in 50mM PIPES (Sigma-Aldrich) pH 7.0. After 20min of
438 incubation in dark, seedlings were washing 3-times in water and placed between slide and
439 lamella. Confocal imaging was performed using a Zeiss LSM700 with 488nm excitation and

440 >530nm emission filters. Images were then processed in the Zeiss LSM Image Browser
441 Program.

442 **Cutin analysis.** Cuticle composition and content was analyzed as previously described
443 [74,75].

444 **TEM analysis.** For transmission electron microscopy analysis, seeds were removed from
445 siliques by removal of the replum tissue with attached seeds. Seeds were high-pressure
446 frozen with a Leica EM-PACT-1 system. Three seeds were inserted into a flat copper carrier,
447 fast-frozen, and cryosubstituted into the Leica AFS1 device. The different freeze-substitution
448 steps were as follows: 54 h at −90°C in acetone solution containing 0.2% glutaraldehyde, 1%
449 osmium tetroxide, and 0.1% uranyl acetate. The temperature was then raised with a step of
450 2°C/h before remaining for 8 hours at -60°C. The temperature was raised again to -30°C for
451 8h00 before being increased to 4°C. Samples were washed three times for 10 min in 100%
452 acetone before embedding in Spurr's resin, which was performed progressively (8 h in 25%
453 Spurr's resin in acetone, 24 h in 50% Spurr's resin in acetone, 24 h in 75% Spurr's resin in
454 acetone, and two times for 12 h in 100% Spurr's resin). Polymerization was performed at
455 70°C for 18 h.
456 Samples were sectioned (65 nm sections) and imaged at 120 kV using an FEI TEM tecnai
457 Spirit with 4 k x 4 k eagle ccd.
458
459 **Generation of micro-array data.** Microarray analysis was carried out at a Transcriptomic
460 Platform, POPS, at the Institute of Plant Sciences Paris-Saclay (IPS2, Orsay, France), using a
461 CATMAv7 array based on AGILENT technology [76]. The CATMAv7 array for the
462 Arabidopsis thaliana genome was made using gene annotations included in FLAGdb++, an
463 integrative database of plant genomes (http://urgv.evry.inra.fr/FLAGdb, [77]). The single high
464 density CATMAv7 microarray slide contains four chambers, each containing 149 916

465 primers. Each 60 bp primer is present in triplicate in each chamber for robust analysis, and as
466 both strands. The array contains 35 754 probes (in triplicate) corresponding to genes
467 annotated in TAIRv8 (among which 476 probes correspond to mitochondrial and chloroplast
468 genes), 1289 probes corresponding to EUGENE software predictions, 658 probes to
469 miRNA/MIRs and 240 control probes.

470 3 independent biological replicates were produced. For each biological repetition and
471 each point, RNA samples were obtained by pooling RNAs from staged siliques containing
472 embryos at the pre-globular to globular, or the young to late heart stage. Total RNA was
473 extracted using the Spectrum^{TM} Plant Total RNA Kit (Sigma-Aldrich) according to the
474 suppliers' instructions. For each comparison, one technical replicate with fluorochrome
475 reversal was performed for each biological replicate (i.e. four hybridizations per comparison).
476 The labelling of cRNAs with Cy3-dUTP or Cy5-dUTP was performed as described in the
477 Two-Color Microarray-Based Gene Expression Analysis Low Input Quick Amp Labeling
478 manual (© Agilent Technologies, Inc.). The hybridization and washing steps were performed
479 according to the Agilent Microarray Hybridization Chamber User Guide instructions ((©
480 Agilent Technologies, Inc.). Two micron scanning was performed with InnoScan900 scanner
481 (Innopsys^{R}, Carbonne, FRANCE) and raw data were extracted using Mapix^{R} software
482 (Innopsys^{R}, Carbonne, FRANCE).

483

484 **Statistical Analysis of Microarray Data.** Experiments were designed with the statistics
485 group of the Unité de Recherche en Génomique Végétale. For each array, the raw data
486 comprised the logarithm of median feature pixel intensity at wavelengths 635 nm (red) and
487 532 nm (green). For each array, a global intensity-dependent normalization using the loess
488 procedure [78] was performed to correct the dye bias. The differential analysis was based on
489 log-ratio averaging over the duplicate probes and over the technical replicates. Hence the

490 number of available data points for each gene equals the number of biological replicates and
491 is used to calculate the moderated t-test [79]. Analysis was carried out using the R software
492 (http://www.R-project.org). Under the null hypothesis, no evidence that the specific variances
493 vary between probes was highlighted by Limma and consequently the moderated t-statistic
494 was assumed to follow a standard normal distribution. To control the false discovery rate,
495 adjusted p-values found using the optimized FDR approach [80] were calculated. We
496 considered as being differentially expressed, the probes with an adjusted p-value ≤ 0.05. The
497 function SqueezeVar of the library Limma was used to smooth the specific variances by
498 computing empirical Bayes posterior means. The library kerfdr was used to calculate the
499 adjusted p-values.
500
501 **Data Deposition.** Microarray data from this article were deposited at Gene Expression
502 Omnibus (http://www.ncbi.nlm.nih.gov/geo/), accession no. GSE68048) and at CATdb
503 (http://urgv.evry.inra.fr/CATdb/; Project: AU14-04_INASEED) according to the "Minimum
504 Information About a Microarray Experiment" standards.
505
506 **Quantitative gene expression analysis in seeds.** Intact siliques were frozen in liquid
507 nitrogen and total RNA was extracted using the Spectrum Plant Total RNA Kit (Sigma). Total
508 RNAs were digested with Turbo DNA-free DNase I (Ambion) according to the
509 manufacturer's instructions. RNA was reverse transcribed using the SuperScript VILO cDNA
510 Synthesis Kit (Invitrogen) according to the manufacturer's protocol. PCR reactions were
511 performed in an optical 384-well plate in the QuantStudio 6 Flex System (Applied
512 Biosystems), using FastStart Universal SYBR Green Master (Rox) (Roche), in a final volume
513 of 10 µl, according to the manufacturer's instructions. The following standard thermal profile
514 was used for all PCR reactions: 95 °C for 10 min, 40 cycles of 95 °C for 10 s, and 60 °C for

515 30 s. Data were analysed using the QuantStudio 6 Flex Real-Time PCR System Software
516 (Applied Biosystems). As a reference, primers for the EIF4A cDNA were used. PCR
517 efficiency (E) was estimated from the data obtained from standard curve amplification using
518 the equation $E=10^{-1/slope}$. Expression levels are presented as $E^{-\Delta Ct}$, where $\Delta Ct=Ct_{GOI}-Ct_{EIF4A}$.
519 Primers are listed in Supplementary Table 2.

520 **Toluidine blue staining.** The lids of plates containing etiolated seedlings were removed and
521 plates were immediately flooded with staining solution [0.05% (w/v) Toluidine Blue + 0.4%
522 (v/v) Tween-20] for 2 minutes. The staining solution was poured off and plates were
523 immediately rinsed gently by flooding under a running tap until the water stream was no
524 longer visibly blue (1-2 minutes). Seedlings were photographed under a Leica MZ12
525 stereomicroscope.

526 **Protein extraction and MPK6 activation analysis.** Seedlings or seeds were quickly frozen
527 in liquid nitrogen and proteins were extracted in buffer containing 50 mM Tris pH 7.5, 200
528 mM NaCl, 1 mM EDTA pH 8, 10% glycerol, 0.1% tween 20, 1 mM phenylmethylsulfonyl
529 fluoride, 1 mM dithiothreitol, 1x protease inhibitor cocktail P9599 (Sigma-Aldrich), and 1x
530 MS-Safe protease and phosphatase inhibitor cocktail (Sigma-Aldrich). Equal amounts of
531 proteins (20 µg for seedlings and 10 µg for seeds) were resolved on 10% polyacrylamide gels
532 and transferred onto a nylon membrane (Schleicher & Schuell). For seedlings primary
533 antibodies against phospho p44/42 MAP kinase (1:2000 dilution) (Cell Signaling
534 Technologies) and then against MPK6 (1:10000 dilution) (Sigma-Aldrich) were used with
535 horseradish peroxidase-conjugated anti-rabbit as secondary antibody. Signal detection was
536 performed using the SuperSignal™ West Femto Maximum Sensitivity Substrate kit (Pierce).
537 For seeds primary antibodies against phospho p44/42 MAP kinase and then against MPK6
538 were used with IRDye® 800CW Donkey anti-Rabbit IgG (H + LI-COR, 1:10000 dilution),
539 and the bound complex was detected using the Odyssey Infrared Imaging System (Li-Cor;

540 Lincoln, NE). The images were analysed and quantified with ImageJ. Background was
541 subtracted for each band. To test the linearity of the detection, 5-15 µg protein from heart
542 stage developing seeds were treated as previously. To detect the antibody against phospho
543 p44/42 MAP kinase an anti-Rabbit IgG, HRP conjugate (Amersham, 1:30000) was used.
544 Anti-alpha-tubulin (Sigma, 1:2000) was used with an anti-mouse IgG, HRP conjugate (GE
545 HealthCare, 1:10000). Signal detection was performed using Clarity Max™ Western ECL
546 Substrate (Biorad) with a ChemiDoc Touch (Biorad) instrument. The images were quantified
547 with ImageJ. Background was subtracted for each band.

548

549 **Acknowledgements**

550 We would like to thank Professor N. Geldner for providing seeds, and A. Lacroix, J. Berger,
551 P, Bolland, H. Leyral and I. Desbouchages for assistance with plant growth and logistics. AC
552 was funded by a grant from the French National Research Agency (ANR-13-BSV2-0002,
553 INASEED). SM was supported by a doctoral grant from the Rhône-Alpes region. RG was
554 supported by a European Research Council Starting Grant (Phymorph #307387). NMD is
555 funded by a PhD fellowship from the Ministère de l'Enseignement Supérieur et de la
556 Recherche. Microscopy and lipid analyses were respectively performed at the Bordeaux
557 Imaging Center (which is a member of the national infrastructure France BioImaging), and
558 the Metabolome Facility of the Functional Genomic Center of Bordeaux (which is supported
559 by the grant MetaboHUB-ANR-11-INBS-0010).

560 **Author contributions**

561 Experiments were carried out by AC, LB, JJ, LT, NMD, SP, SM, ACM and FD. Results were
562 analyzed by all authors. GI, FD, JJ, TW and RG designed experiments and supervised the
563 work. GI wrote the paper with contributions from all authors.

564 **The authors declare that they have no competing financial interests.**

565 **Figure Legends**

566 **Figure 1**

567 **Genes involved in cuticle biosynthesis are co-expressed with *GSO1* and *GSO2* during**
568 **embryogenesis, but their expression is not dependent upon GSO1 and GSO2.** Analysis of
569 the expression of genes involved in cuticle biosynthesis in wild-type (Col-0) and *gso1-1 gso2-*
570 *1* seeds containing late globular/triangle, heart and early torpedo stage embryos (left to right).

571 **Figure 2**

572 **Localisation and functionality of the *pGSO1:GSO1-mVENUS transgene* in developing**
573 **embryos.** Confocal images of GSO1-mVENUS at early heart, mid heart, late heart and early
574 torpedo stages of development (a-d). (e) The *pGSO1:GSO1-mVENUS* transgene complements
575 seedling cuticle defects in *gso1-1 gso2-1* double mutants. Quantification of seedling toluidine
576 blue permeability was carried out as described in Moussu et al., 2017. Error bars represent
577 standard errors from three biological replicates. (f-h) The *pGSO1-GSO1:mVENUS* transgene
578 complements seed shape defects in *gso1-1 gso2-1* double mutants. Seed populations from
579 wild-type (f), *gso1-1 gso2-1* double mutants (g) and *gso1-1 gso2-1* double mutants carrying
580 the *pGSO1:GSO1-mVENUS* transgene (h). Occasional misshapen shaped seeds are observed
581 in the complemented line (white arrows), compared with nearly 100% misshapen seeds in the
582 un-complemented double mutant. Scale bar = 1mm.

583 **Figure 3**

584 **Cuticle permeability defects in *ale1-4* and *gso1-1 gso2-1* seedlings do not correlate with**
585 **changes in cutin load.** (a) Cotyledons grown *in vitro* for 5 days under continuous light were
586 collected, delipidated and their cutin content and composition was analyzed as described in

587 the Material and Method section. ωOH and DCA stand respectively for omega-hydroxy acid
588 and α,ω-dicarboxylic acid. Mean values are shown in µg/mg of delipidated dry residue (DR)
589 ± SD of three replicates. Statistical differences were determined according to a Student's *t* test
590 : *** denotes p<0.0001, ** denotes p<0.001 and * denotes p<0.01. (b) Cuticle permeability to
591 toluidine blue in etiolated seedlings from the genotypes tested in (a).

592 **Figure 4**

593 **Embryonic cuticle biogenesis involves a process of patch coalescence that is defective in**
594 ***ale1-4* and *gso1-1 gso2-1* mutants.** Analysis of embryonic cuticle deposition in wild-type (a-
595 d), *gso1-1 gso2-1* (e-f) and *ale1-4* (g,h) embryos at 2 cell (a), mid globular (b), mid heart
596 (c,e,g) and walking stick (d,f,h) stages of embryogenesis. White arrows show the external face
597 of the embryonic cuticle. Scale bar = 500nm.

598 **Figure 5**

599 **ALE1, GSO1 and GSO2 positively regulate the expression of stress-related genes in**
600 **seeds.** (a) Summary of overlaps between gene sets showing reduced expression in *ale1-4* and
601 *gso1-1 gso2-1* mutants at the globular and heart stages of development. (b) GO term analysis
602 of genes down-regulated in both *ale1-4* and *gso1-1 gso2-2* mutants at the heart stage.

603 **Figure 6**

604 **MPK6 acts downstream of ALE1, GSO1 and GSO2 mediated signalling.** (a) Seedling
605 cuticle permeability phenotypes of *mpk6-2* and *ale1-4* and *gso1-1 gso2-1* mutants and in
606 double and triple mutant combinations. Scale bar = 2mm (b) Analysis of proteins extracted
607 from developing seeds at the globular-early torpedo stage. The mutants *mpk3-1* and *mpk6-2*
608 were included to confirm band identification. No phosphorylation of MPKs other than MPK6
609 is observed in Col-0, *gso1-1 gso2-1* or *mpk3-1* seeds, but an additional band (**) is

610 systematically observed in the *mpk6-2* mutant background. * Indicates a non specific band
611 detected by the anti-MPK6 antibody. This experiment was repeated 7 times on independent
612 biological samples, with similar results. (c) Degree of phosphorylation of MPK6 in Col-0 and
613 *gso1-1 gso2-1* mutant seeds. Error bars represent SD of 3 biological replicates (see
614 Supplementary Figure 16 for linearity testing).

615 **Figure 7**

616 **MPK6 activity is required in the embryo and testa, but not the endosperm, for normal**
617 **seedling development.** (a) Representative phenotypes of toluidine blue-stained seedlings
618 from wild-type (Col-0), *mpk6-2,* and these backgrounds transformed with *pRGP3-MPK6* or
619 *pRPS5A-MPK6.* Lines correspond to those described in Supplementary Figure 17. Scale bar =
620 2mm

621 **References**

622 1. Ingram GC (2010) Family life at close quarters: communication and constraint in angiosperm seed
623 development. Protoplasma 247: 195-214.
624 2. Baroux C, Spillane C, Grossniklaus U (2002) Evolutionary origins of the endosperm in flowering
625 plants. Genome Biol 3: reviews1026.
626 3. Fiume E, Fletcher JC (2012) Regulation of Arabidopsis embryo and endosperm development by the
627 polypeptide signaling molecule CLE8. Plant Cell 24: 1000-1012.
628 4. Costa LM, Marshall E, Tesfaye M, Silverstein KA, Mori M, et al. (2014) Central cell-derived peptides
629 regulate early embryo patterning in flowering plants. Science 344: 168-172.
630 5. Bayer M, Nawy T, Giglione C, Galli M, Meinnel T, et al. (2009) Paternal control of embryonic
631 patterning in Arabidopsis thaliana. Science 323: 1485-1488.
632 6. Pfister A, Barberon M, Alassimone J, Kalmbach L, Lee Y, et al. (2014) A receptor-like kinase mutant
633 with absent endodermal diffusion barrier displays selective nutrient homeostasis defects.
634 Elife 3: e03115.
635 7. Xing Q, Creff A, Waters A, Tanaka H, Goodrich J, et al. (2013) ZHOUPI controls embryonic cuticle
636 formation via a signalling pathway involving the subtilisin protease ABNORMAL LEAF-SHAPE1
637 and the receptor kinases GASSHO1 and GASSHO2. Development 140: 770-779.
638 8. Yang S, Johnston N, Talideh E, Mitchell S, Jeffree C, et al. (2008) The endosperm-specific ZHOUPI
639 gene of Arabidopsis thaliana regulates endosperm breakdown and embryonic epidermal
640 development. Development 135: 3501-3509.
641 9. Tsuwamoto R, Fukuoka H, Takahata Y (2008) GASSHO1 and GASSHO2 encoding a putative leucine-
642 rich repeat transmembrane-type receptor kinase are essential for the normal development
643 of the epidermal surface in Arabidopsis embryos. Plant J 54: 30-42.

644 10. Tanaka H, Onouchi H, Kondo M, Hara-Nishimura I, Nishimura M, et al. (2001) A subtilisin-like
645 serine protease is required for epidermal surface formation in Arabidopsis embryos and
646 juvenile plants. Development 128: 4681-4689.
647 11. Moussu S, San-Bento R, Galletti R, Creff A, Farcot E, et al. (2013) Embryonic cuticle establishment:
648 the great (apoplastic) divide. Plant Signal Behav 8: e27491.
649 12. San-Bento R, Farcot E, Galletti R, Creff A, Ingram G (2014) Epidermal identity is maintained by
650 cell-cell communication via a universally active feedback loop in Arabidopsis thaliana. Plant J
651 77: 46-58.
652 13. Bernard A, Joubes J (2012) Arabidopsis cuticular waxes: Advances in synthesis, export and
653 regulation. Prog Lipid Res 52: 110-129.
654 14. Fich EA, Segerson NA, Rose JK (2016) The Plant Polyester Cutin: Biosynthesis, Structure, and
655 Biological Roles. Annu Rev Plant Biol 10.1146/annurev-arplant-043015-111929.
656 15. Javelle M, Vernoud V, Rogowsky PM, Ingram GC (2011) Epidermis: the formation and functions of
657 a fundamental plant tissue. New Phytol 189: 17-39.
658 16. Serrano M, Coluccia F, Torres M, L'Haridon F, Metraux JP (2014) The cuticle and plant defense to
659 pathogens. Front Plant Sci 5: 274.
660 17. Tanaka T, Tanaka H, Machida C, Watanabe M, Machida Y (2004) A new method for rapid
661 visualization of defects in leaf cuticle reveals five intrinsic patterns of surface defects in
662 Arabidopsis. Plant J 37: 139-146.
663 18. Delude C, Moussu S, Joubes J, Ingram G, Domergue F (2016) Plant Surface Lipids and Epidermis
664 Development. Sub-cellular biochemistry 86: 287-313.
665 19. Le BH, Cheng C, Bui AQ, Wagmaister JA, Henry KF, et al. (2010) Global analysis of gene activity
666 during Arabidopsis seed development and identification of seed-specific transcription
667 factors. Proc Natl Acad Sci U S A 107: 8063-8070.
668 20. Winter D, Vinegar B, Nahal H, Ammar R, Wilson GV, et al. (2007) An "Electronic Fluorescent
669 Pictograph" browser for exploring and analyzing large-scale biological data sets. PLoS One 2:
670 e718.
671 21. Belmonte MF, Kirkbride RC, Stone SL, Pelletier JM, Bui AQ, et al. (2013) Comprehensive
672 developmental profiles of gene activity in regions and subregions of the Arabidopsis seed.
673 Proc Natl Acad Sci U S A 110: E435-444.
674 22. Lu S, Song T, Kosma DK, Parsons EP, Rowland O, et al. (2009) Arabidopsis CER8 encodes LONG-
675 CHAIN ACYL-COA SYNTHETASE 1 (LACS1) that has overlapping functions with LACS2 in plant
676 wax and cutin synthesis. Plant J 59: 553-564.
677 23. Schnurr J, Shockey J, Browse J (2004) The acyl-CoA synthetase encoded by LACS2 is essential for
678 normal cuticle development in Arabidopsis. Plant Cell 16: 629-642.
679 24. Li-Beisson Y, Shorrosh B, Beisson F, Andersson MX, Arondel V, et al. (2013) Acyl-lipid metabolism.
680 Arabidopsis Book 11: e0161.
681 25. Beisson F, Li-Beisson Y, Pollard M (2012) Solving the puzzles of cutin and suberin polymer
682 biosynthesis. Curr Opin Plant Biol 15: 329-337.
683 26. Pruitt RE, Vielle-Calzada JP, Ploense SE, Grossniklaus U, Lolle SJ (2000) FIDDLEHEAD, a gene
684 required to suppress epidermal cell interactions in Arabidopsis, encodes a putative lipid
685 biosynthetic enzyme. Proc Natl Acad Sci U S A 97: 1311-1316.
686 27. Yephremov A, Wisman E, Huijser P, Huijser C, Wellesen K, et al. (1999) Characterization of the
687 FIDDLEHEAD gene of Arabidopsis reveals a link between adhesion response and cell
688 differentiation in the epidermis. The Plant Cell 11: 2187-2201.
689 28. Wellesen K, Durst F, Pinot F, Benveniste I, Nettesheim K, et al. (2001) Functional analysis of the
690 LACERATA gene of Arabidopsis provides evidence for different roles of fatty acid omega -
691 hydroxylation in development. Proc Natl Acad Sci U S A 98: 9694-9699.
692 29. Kurdyukov S, Faust A, Nawrath C, Bar S, Voisin D, et al. (2006) The epidermis-specific extracellular
693 BODYGUARD controls cuticle development and morphogenesis in Arabidopsis. Plant Cell 18:
694 321-339.

695 30. Debono A, Yeats TH, Rose JK, Bird D, Jetter R, et al. (2009) Arabidopsis LTPG Is a
696 Glycosylphosphatidylinositol-Anchored Lipid Transfer Protein Required for Export of Lipids to
697 the Plant Surface. Plant Cell.
698 31. Bird D, Beisson F, Brigham A, Shin J, Greer S, et al. (2007) Characterization of Arabidopsis
699 ABCG11/WBC11, an ATP binding cassette (ABC) transporter that is required for cuticular lipid
700 secretion. Plant J 52: 485-498.
701 32. Li Y, Beisson F, Koo AJ, Molina I, Pollard M, et al. (2007) Identification of acyltransferases required
702 for cutin biosynthesis and production of cutin with suberin-like monomers. Proc Natl Acad Sci
703 U S A 104: 18339-18344.
704 33. Sarnowski TJ, Rios G, Jasik J, Swiezewski S, Kaczanowski S, et al. (2005) SWI3 subunits of putative
705 SWI/SNF chromatin-remodeling complexes play distinct roles during Arabidopsis
706 development. Plant Cell 17: 2454-2472.
707 34. Shiu SH, Bleecker AB (2001) Receptor-like kinases from Arabidopsis form a monophyletic gene
708 family related to animal receptor kinases. Proc Natl Acad Sci U S A 98: 10763-10768.
709 35. Shiu SH, Bleecker AB (2003) Expansion of the receptor-like kinase/Pelle gene family and receptor-
710 like proteins in Arabidopsis. Plant Physiol 132: 530-543.
711 36. Yamaguchi Y, Huffaker A, Bryan AC, Tax FE, Ryan CA (2010) PEPR2 is a second receptor for the
712 Pep1 and Pep2 peptides and contributes to defense responses in Arabidopsis. Plant Cell 22:
713 508-522.
714 37. Krol E, Mentzel T, Chinchilla D, Boller T, Felix G, et al. (2010) Perception of the Arabidopsis danger
715 signal peptide 1 involves the pattern recognition receptor AtPEPR1 and its close homologue
716 AtPEPR2. J Biol Chem 285: 13471-13479.
717 38. Yamaguchi Y, Huffaker A (2011) Endogenous peptide elicitors in higher plants. Curr Opin Plant
718 Biol 14: 351-357.
719 39. Lopez-Bucio JS, Dubrovsky JG, Raya-Gonzalez J, Ugartechea-Chirino Y, Lopez-Bucio J, et al. (2014)
720 Arabidopsis thaliana mitogen-activated protein kinase 6 is involved in seed formation and
721 modulation of primary and lateral root development. J Exp Bot 65: 169-183.
722 40. Zhang M, Wu H, Su J, Wang H, Zhu Q, et al. (2017) Maternal control of embryogenesis by MPK6
723 and its upstream MKK4/MKK5 in Arabidopsis. Plant J 92: 1005-1019.
724 41. Moussu S, Doll NM, Chamot S, Brocard L, Creff A, et al. (2017) ZHOUPI and KERBEROS Mediate
725 Embryo/Endosperm Separation by Promoting the Formation of an Extracuticular Sheath at
726 the Embryo Surface. Plant Cell 29: 1642-1656.
727 42. Zhang Y, Wang P, Shao W, Zhu JK, Dong J (2015) The BASL polarity protein controls a MAPK
728 signaling feedback loop in asymmetric cell division. Dev Cell 33: 136-149.
729 43. Sethi V, Raghuram B, Sinha AK, Chattopadhyay S (2014) A mitogen-activated protein kinase
730 cascade module, MKK3-MPK6 and MYC2, is involved in blue light-mediated seedling
731 development in Arabidopsis. Plant Cell 26: 3343-3357.
732 44. Smekalova V, Luptovciak I, Komis G, Samajova O, Ovecka M, et al. (2014) Involvement of YODA
733 and mitogen activated protein kinase 6 in Arabidopsis post-embryogenic root development
734 through auxin up-regulation and cell division plane orientation. New Phytol 203: 1175-1193.
735 45. Guan Y, Meng X, Khanna R, LaMontagne E, Liu Y, et al. (2014) Phosphorylation of a WRKY
736 transcription factor by MAPKs is required for pollen development and function in
737 Arabidopsis. PLoS Genet 10: e1004384.
738 46. Guan Y, Lu J, Xu J, McClure B, Zhang S (2014) Two Mitogen-Activated Protein Kinases, MPK3 and
739 MPK6, Are Required for Funicular Guidance of Pollen Tubes in Arabidopsis. Plant Physiol 165:
740 528-533.
741 47. Jewaria PK, Hara T, Tanaka H, Kondo T, Betsuyaku S, et al. (2013) Differential effects of the
742 peptides Stomagen, EPF1 and EPF2 on activation of MAP kinase MPK6 and the SPCH protein
743 level. Plant Cell Physiol 54: 1253-1262.
744 48. Khan M, Rozhon W, Bigeard J, Pflieger D, Husar S, et al. (2013) Brassinosteroid-regulated
745 GSK3/Shaggy-like kinases phosphorylate mitogen-activated protein (MAP) kinase kinases,
746 which control stomata development in Arabidopsis thaliana. J Biol Chem 288: 7519-7527.

747 49. Meng X, Wang H, He Y, Liu Y, Walker JC, et al. (2012) A MAPK cascade downstream of ERECTA
748 receptor-like protein kinase regulates Arabidopsis inflorescence architecture by promoting
749 localized cell proliferation. Plant Cell 24: 4948-4960.
750 50. Muller J, Beck M, Mettbach U, Komis G, Hause G, et al. (2010) Arabidopsis MPK6 is involved in cell
751 division plane control during early root development, and localizes to the pre-prophase
752 band, phragmoplast, trans-Golgi network and plasma membrane. Plant J 61: 234-248.
753 51. Cho SK, Larue CT, Chevalier D, Wang H, Jinn TL, et al. (2008) Regulation of floral organ abscission
754 in Arabidopsis thaliana. Proc Natl Acad Sci U S A 105: 15629-15634.
755 52. Wang H, Liu Y, Bruffett K, Lee J, Hause G, et al. (2008) Haplo-insufficiency of MPK3 in MPK6
756 mutant background uncovers a novel function of these two MAPKs in Arabidopsis ovule
757 development. Plant Cell 20: 602-613.
758 53. Ren D, Liu Y, Yang KY, Han L, Mao G, et al. (2008) A fungal-responsive MAPK cascade regulates
759 phytoalexin biosynthesis in Arabidopsis. Proc Natl Acad Sci U S A 105: 5638-5643.
760 54. Moussu SA, Doll NM, Chamot S, Brocard L, Creff A, et al. (2017) ZHOUPI and KERBEROS Mediate
761 Embryo/Endosperm Separation by Promoting the Formation of an Extra-Cuticular Sheath at
762 the Embryo Surface. Plant Cell 10.1105/tpc.17.00016.
763 55. Denay G, Creff A, Moussu S, Wagnon P, Thevenin J, et al. (2014) Endosperm breakdown in
764 Arabidopsis requires heterodimers of the basic helix-loop-helix proteins ZHOUPI and
765 INDUCER OF CBP EXPRESSION 1. Development 141: 1222-1227.
766 56. Bartels S, Lori M, Mbengue M, van Verk M, Klauser D, et al. (2013) The family of Peps and their
767 precursors in Arabidopsis: differential expression and localization but similar induction of
768 pattern-triggered immune responses. J Exp Bot 64: 5309-5321.
769 57. Postel S, Kufner I, Beuter C, Mazzotta S, Schwedt A, et al. (2010) The multifunctional leucine-rich
770 repeat receptor kinase BAK1 is implicated in Arabidopsis development and immunity. Eur J
771 Cell Biol 89: 169-174.
772 58. Kim BH, Kim SY, Nam KH (2013) Assessing the diverse functions of BAK1 and its homologs in
773 arabidopsis, beyond BR signaling and PTI responses. Molecules and cells 35: 7-16.
774 59. Lee Y, Rubio MC, Alassimone J, Geldner N (2013) A mechanism for localized lignin deposition in
775 the endodermis. Cell 153: 402-412.
776 60. Steinhorst L, Kudla J (2013) Calcium and reactive oxygen species rule the waves of signaling. Plant
777 Physiol 163: 471-485.
778 61. Kadota Y, Shirasu K, Zipfel C (2015) Regulation of the NADPH Oxidase RBOHD During Plant
779 Immunity. Plant Cell Physiol 56: 1472-1480.
780 62. Dominguez E, Heredia-Guerrero JA, Heredia A (2015) Plant cutin genesis: unanswered questions.
781 Trends Plant Sci 20: 551-558.
782 63. Liu Y, He C (2017) A review of redox signaling and the control of MAP kinase pathway in plants.
783 Redox Biol 11: 192-204.
784 64. Jalmi SK, Sinha AK (2015) ROS mediated MAPK signaling in abiotic and biotic stress- striking
785 similarities and differences. Front Plant Sci 6: 769.
786 65. Ellinger D, Voigt CA (2014) Callose biosynthesis in Arabidopsis with a focus on pathogen response:
787 what we have learned within the last decade. Annals of botany 114: 1349-1358.
788 66. Voigt CA (2014) Callose-mediated resistance to pathogenic intruders in plant defense-related
789 papillae. Front Plant Sci 5: 168.
790 67. Tang D, Simonich MT, Innes RW (2007) Mutations in LACS2, a long-chain acyl-coenzyme A
791 synthetase, enhance susceptibility to avirulent Pseudomonas syringae but confer resistance
792 to Botrytis cinerea in Arabidopsis. Plant Physiology 144: 1093-1103.
793 68. Xiao F, Goodwin SM, Xiao Y, Sun Z, Baker D, et al. (2004) Arabidopsis CYP86A2 represses
794 Pseudomonas syringae type III genes and is required for cuticle development. EMBO J 23:
795 2903-2913.
796 69. Waters A, Creff A, Goodrich J, Ingram G (2013) "What we've got here is failure to communicate":
797 Zou mutants and endosperm cell death in seed development. Plant Signal Behav 8.

798 70. Pearce G, Yamaguchi Y, Barona G, Ryan CA (2010) A subtilisin-like protein from soybean contains
799 an embedded, cryptic signal that activates defense-related genes. Proc Natl Acad Sci U S A
800 107: 14921-14925.
801 71. Ramirez V, Lopez A, Mauch-Mani B, Gil MJ, Vera P (2013) An extracellular subtilase switch for
802 immune priming in Arabidopsis. PLoS Pathog 9: e1003445.
803 72. Nakayama T, Shinohara H, Tanaka M, Baba K, Ogawa-Ohnishi M, et al. (2017) A peptide hormone
804 required for Casparian strip diffusion barrier formation in Arabidopsis roots. Science 355:
805 284-286.
806 73. Doblas VG, Smakowska-Luzan E, Fujita S, Alassimone J, Barberon M, et al. (2017) Root diffusion
807 barrier control by a vasculature-derived peptide binding to the SGN3 receptor. Science 355:
808 280-284.
809 74. Domergue F, Vishwanath SJ, Joubes J, Ono J, Lee JA, et al. (2010) Three Arabidopsis fatty acyl-
810 coenzyme A reductases, FAR1, FAR4, and FAR5, generate primary fatty alcohols associated
811 with suberin deposition. Plant Physiol 153: 1539-1554.
812 75. Bourdenx B, Bernard A, Domergue F, Pascal S, Leger A, et al. (2011) Overexpression of
813 Arabidopsis ECERIFERUM1 promotes wax very-long-chain alkane biosynthesis and influences
814 plant response to biotic and abiotic stresses. Plant Physiol 156: 29-45.
815 76. Gagnot S, Tamby JP, Martin-Magniette ML, Bitton F, Taconnat L, et al. (2008) CATdb: a public
816 access to Arabidopsis transcriptome data from the URGV-CATMA platform. Nucleic Acids Res
817 36: D986-990.
818 77. Derozier S, Samson F, Tamby JP, Guichard C, Brunaud V, et al. (2011) Exploration of plant
819 genomes in the FLAGdb++ environment. Plant Methods 7: 8.
820 78. Yang YH, Dudoit S, Luu P, Lin DM, Peng V, et al. (2002) Normalization for cDNA microarray data: a
821 robust composite method addressing single and multiple slide systematic variation. Nucleic
822 Acids Res 30: e15.
823 79. Smyth GK (2004) Linear models and empirical bayes methods for assessing differential expression
824 in microarray experiments. Statistical applications in genetics and molecular biology 3:
825 Article3.
826 80. Storey JD, Tibshirani R (2003) Statistical significance for genomewide studies. Proc Natl Acad Sci U
827 S A 100: 9440-9445.

828

829 **Supporting Information Legends**

830 **Supplementary Figure 1 (Related to Figure 1) : Genes involved in cuticle biosynthesis**
831 **are expressed early during embryo development and are co-expressed with *GSO1* and**
832 ***GSO2*.** Expression data for *LACS2* **(a)**, *FDH* **(b)**, *BDG* **(c)**, *LCR* **(d)**, *LTPG1* **(e)**, *ABCG11* **(f)**,
833 *GSO1* **(g)** and *GSO2* **(h)** downloaded from the Seed Gene Network resource
834 (http://seedgenenetwork.net/).

835 **Supplementary Figure 2 (Related to Figure 1) : Genes involved in cuticle biosynthesis**
836 **are co-expressed with *GSO1* and *GSO2* in the embryonic epidermis during**
837 **embryogenesis, but their expression is not dependent upon GSO1 and GSO2.** Analysis

838 of the expression of genes involved in cuticle biosynthesis in wild-type (Col-0) and *gso1-1*
839 *gso2-1* seeds containing late globular/triangle, heart and early torpedo stage embryos (left to
840 right).

841 **Supplementary Figure 3 (Related to Figure 1) : Hybridization of tissue sections to an**
842 **antisense *GFP* probe as negative control in Col-0 (a-c) and *gso1 gso2* (d-f) seeds**
843 **containing late globular (a,d), heart (b,e) and early torpedo (c,f) stage embryos.**
844 Expression of *LTPG1* in wild type seed containing torpedo stage embryo is shown in (g) for
845 direct comparison.

846 **Supplementary Figure 4 (Related to Figure 4) : Analysis of the permeability of**
847 **extruded Col-0 embryos at different developmental stages to toluidine blue treatment.**
848 Three stained and one unstained embryo (below) are shown for each developmental stage.
849 Scale bar = 100mm

850 **Supplementary Figure 5 (Related to Figure 4) : Cuticle discontinuities in early wild-**
851 **type (Col-0) embryos and later *gso1 gso2* embryos. a,b)** Cuticle the mid-late globular
852 stage (during gap closure) in Col-0 embryos showing disconuinuous cuticle. *gso1-1 gso2-1*
853 mutant embryos maintain a diffuse and discontinuous cuticle at later stages. Analysis of
854 embryonic cuticle deposition in *gso1-1 gso2-1* at the *mid heart* **(c-d)** and walking stick **(e-f)**
855 stages of embryogenesis, when wild-type cuticle is continuous. White arrows show external
856 face of embryonic cuticle. Scale bar = 500nm.

857 **Supplementary Figure 6 (Related to Figure 5) : GO term analysis of genes showing**
858 **increased expression in siliques of both *gso1-1 gso2-1* and *ale1-4* mutant**
859 **backgrounds at the globular (a) and heart (b) stages of embryo development.** The
860 degree of overlap between these datasets is illustrated in **(c)**.

861 **Supplementary Figure 7 (Related to Figure 5) : GO term analysis of genes showing**
862 **reduced expression in siliques of both *gso1-1 gso2-1* and *ale1-4* mutant backgrounds**
863 **at the globular (a) and heart (b) stages of embryo development.**

864 **Supplementary Figure 8 (Related to Figure 5) : Validation by qRT-PCR of microarray**
865 **data.** Experiments were carried out in 4 biological replicates. Values are expressed relative
866 to the *EIF4A* gene. Significance values indicated were calculated using a Student's t-test. ***
867 denotes p<0.01, ** denotes p<0.05 and * denotes p<0.1. Bars indicate standard errors.

868 **Supplementary Figure 9 (Related to Figure 5) : Analysis of the expression of *SWI3A* in**
869 **wild-type (a-c), *gso1-1 gso2-1* (d-f) mutant embryos in seeds containing late**
870 **globular/triangle (a,d), heart (b,e) and early torpedo (c,f) stage embryos.** Expression
871 data for *SWI3A* downloaded from the Seed Gene Network resource
872 (http://seedgenenetwork.net/) is shown in **(g).**

873 **Supplementary Figure 10 (Related to Figure 6) : Non additivity of seed twisting (a-b)**
874 **and seedling cuticle permeability (c) phenotypes between *mpk6-2* and *ale1-4* mutants**
875 **and between *mpk6-2* and *gso1-1 gso2-1* double mutants.** Populations of seeds **(a)** from
876 single double and triple mutants were photographed, and seed phenotypes were quantified
877 **(b)**(Col-0 n= 196, *ale1-4* n=200, *mpk6-2* n=210, *gso1-1 gso2-1* n=111, *mpk6-2 ale1-4* (3
878 individuals) n = 211, 212 and 238, *mpk6-2 gso1-1 gso2-1* n=86). Etiolated seedlings were
879 treated with toluidine blue and seedling and toluidine blue phenotypes were quantified **(c)**.
880 Results are representative of three independent experiments. Col-0 n=389, *ale1-4* n=387 ,
881 *mpk6-2* n=383, *mpk6-2 ale1-4* n=398. (Quantifications were not possible for *mpk6-2 gso1-1*
882 *gso2-1* triple mutants due to low seed set).

883 **Supplementary Figure 11 (Related to Figure 6) : Cuticle phenotypes using Nile-Red**
884 **staining of etiolated cotyledons.** Genotypes are indicated on left panels with zones
885 magnified on the right highlighted by white boxes. Arrows indicate position of the cuticle and
886 arrowheads indicate gaps in the cuticle. a) Biological replicate 1.

887 **Cuticle phenotypes using Nile-Red staining of etiolated cotyledons.** b) Biological
888 replicate 2

889 **Supplementary Figure 13 (Related to Figure 6) : qRT-PCR analysis of the expression of**
890 **candidate target genes in *mpk6-2* mutant siliques.** Experiments were carried out in
891 biological triplicate. Values are expressed relative to *EIF4* gene expression. Significance
892 values indicated were calculated using a Student's t-test. *** denotes p<0.01, **denotes
893 p<0.05 and * denotes p<0.1. Bars indicate standard errors.

894 **Supplementary Figure 14 (Related to Figure 6) : GSO1 and GSO2 are not necessary for**
895 **MPK6 phosphorylation in response to PAMP-elicitation in seedlings.** Western blot
896 analysis of phosphorylated MPK proteins (upper panel) and then total MPK6 protein (middle
897 panel). Loading control (Ponceau S-stained Rubisco) is shown in lower panel. The same
898 blot is shown in the upper middle and lower panel. * Indicates a non specific band detected
899 by the anti-MPK6 antibody. Seedlings were treated with water or with 100nM flg22 for either
900 15 or 60 minutes before protein extraction. The mutants *mpk3-1* and *mpk6-2* were included
901 to confirm band identities.

902 **Supplementary Figure 15 (Related to Figure 6) : *gso1 gso2* mutant seedlings are not**
903 **significantly affected in the MPK6 phosphorylation response to flg22.** Western blot
904 analysis of phosphorylated MPK proteins (upper panels) and then total MPK6 protein (middle
905 panels). Loading control (Ponceau S-stained Rubisco) is shown in lower panel. The same
906 blot is shown in the upper middle and lower panel. * Indicates a non specific band detected
907 by the anti-MPK6 antibody. Seedlings were treated with water or with 1nM flg22 for either 15
908 or 60 minutes before protein extraction.

909 **Supplementary Figure 16 (Related to Figure 6) : Developing *gso1 gso2* mutant seeds**
910 **show reduced levels of MPK6 phosphorylation compared to wild-type seeds.** a)
911 Western blot analysis of phosphorylated MPK6 protein in developing seeds exposed at four
912 consecutive one minute intervals (to confirm signal linearity). Loading control (α-tubulinA) is
913 shown in lower panel. B) Degree of phosphorylation of MPK6 in Col-0 and *gso1-1 gso2-1*
914 mutant seeds. Error bars represent SD of 3 biological replicates.

915 **Supplementary Figure 17 (Related to Figure 7) : MPK6 is required in the embryo and**
916 **testa, but not the endosperm (a)** Representative phenotypes of seeds from wild-type (Col-
917 0), *mpk6-2,* and these backgrounds transformed with *pRGP3-MPK6 or pRPS5A-MPK6.* **(b)**
918 Quantification of seed phenotypes in the above material. Seeds from at least two
919 independent transgenic lines have been quantified.

920
921
922
923
924
925
926

927

Figure 1

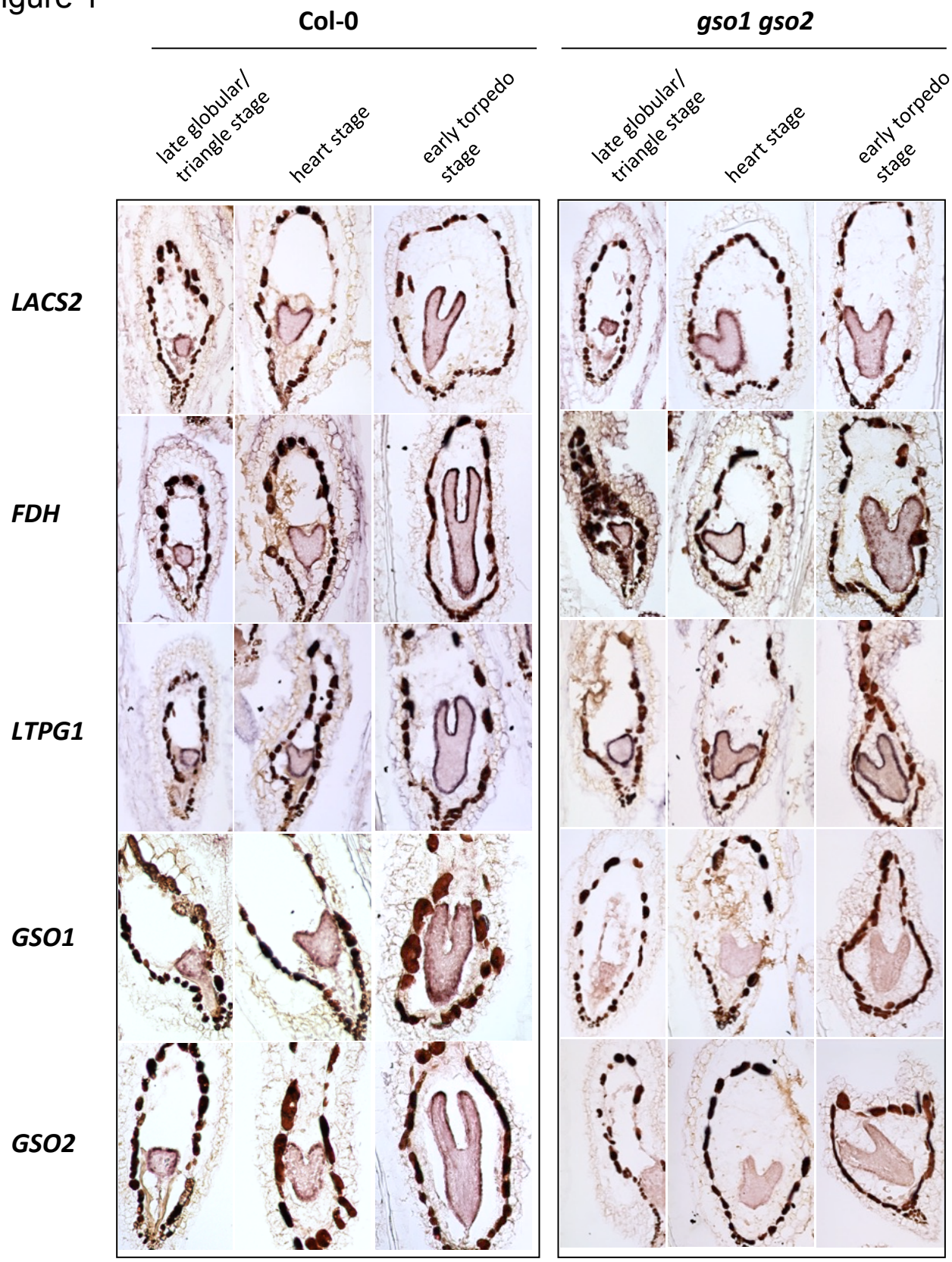

Figure 1

Genes involved in cuticle biosynthesis are co-expressed with *GSO1* and *GSO2* during embryogenesis, but their expression is not dependent upon GSO1 and GSO2. Analysis of the expression of genes involved in cuticle biosynthesis in wild-type (Col-0) and *gso1-1 gso2-1* seeds containing late globular/triangle, heart and early torpedo stage embryos (left to right).

Figure 2

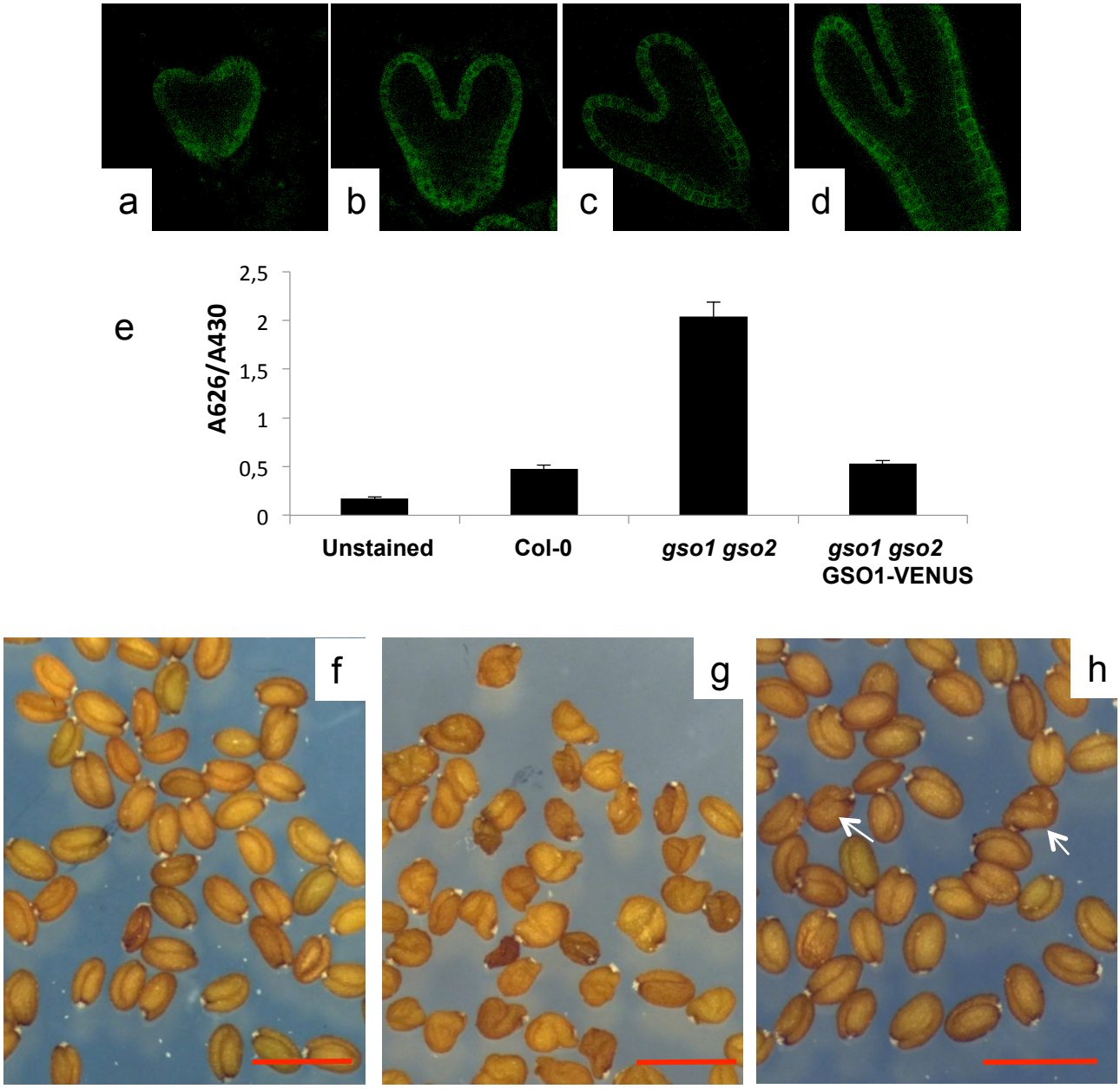

Figure 2

Localisation and functionality of the *pGSO1:GSO1-mVENUS transgene* in developing embryos. Confocal images of GSO1-mVENUS at early heart, mid heart, late heart and early torpedo stages of development (a-d). (e) The *pGSO1:GSO1-mVENUS* transgene complements seedling cuticle defects in *gso1-1 gso2-1* double mutants. Quantification of seedling toluidine blue permeability was carried out as described in Moussu et al., 2017. Error bars represent standard errors from three biological replicates. (f-h) The *pGSO1:GSO1-mVENUS* transgene complements seed shape defects in *gso1-1 gso2-1* double mutants. Seed populations from wild-type (f), *gso1-1 gso2-1* double mutants (g) and *gso1-1 gso2-1* double mutants carrying the The *pGSO1:GSO1-mVENUS* transgene (h). Occasional misshapen shaped seeds are observed in the complemented line (white arrows), compared with 100% misshapen seeds in the un-complemented double mutant. Scale bar = 1mm.

Figure 3

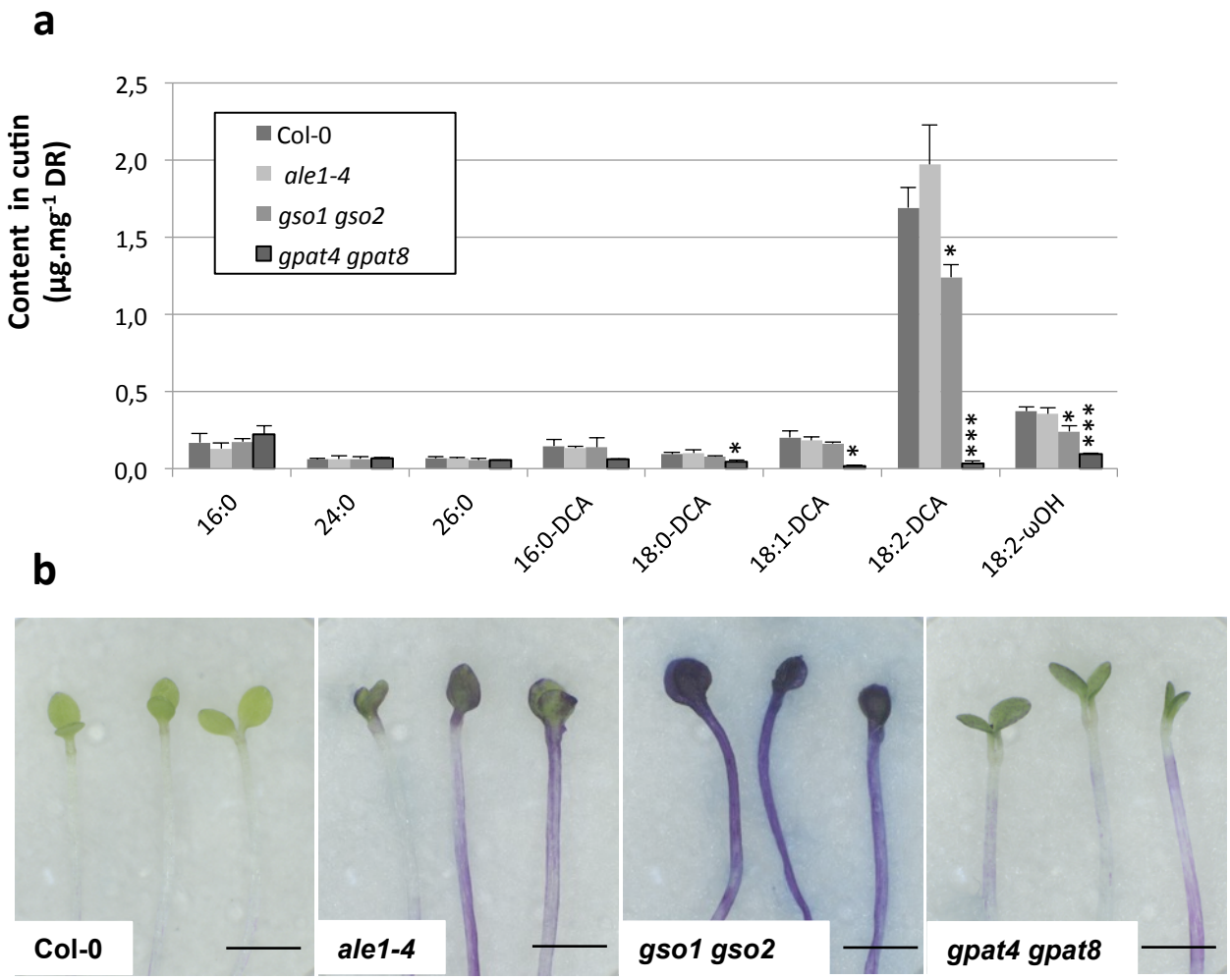

Figure 3

Cuticle permeability defects in *ale1-4* and *gso1-1 gso2-1* seedlings do not correlate with changes in cutin load. (a) Cotyledons grown *in vitro* for 5 days under continuous light were collected, delipidated and their cutin content and composition was analyzed as described in the Material and Method section. ωOH and DCA stand respectively for omega-hydroxy acid and α,ω-dicarboxylic acid. Mean values are shown in µg/mg of delipidated dry residue (DR) ± SD of three replicates. Statistical differences were determined according to a Student's *t* test : *** denotes p<0.0001, ** denotes p<0.001 and * denotes p<0.01. (b) Cuticle permeability to toluidine blue in etiolated seedlings from the genotypes tested in (a). Scale bar = 2mm.

Figure 4

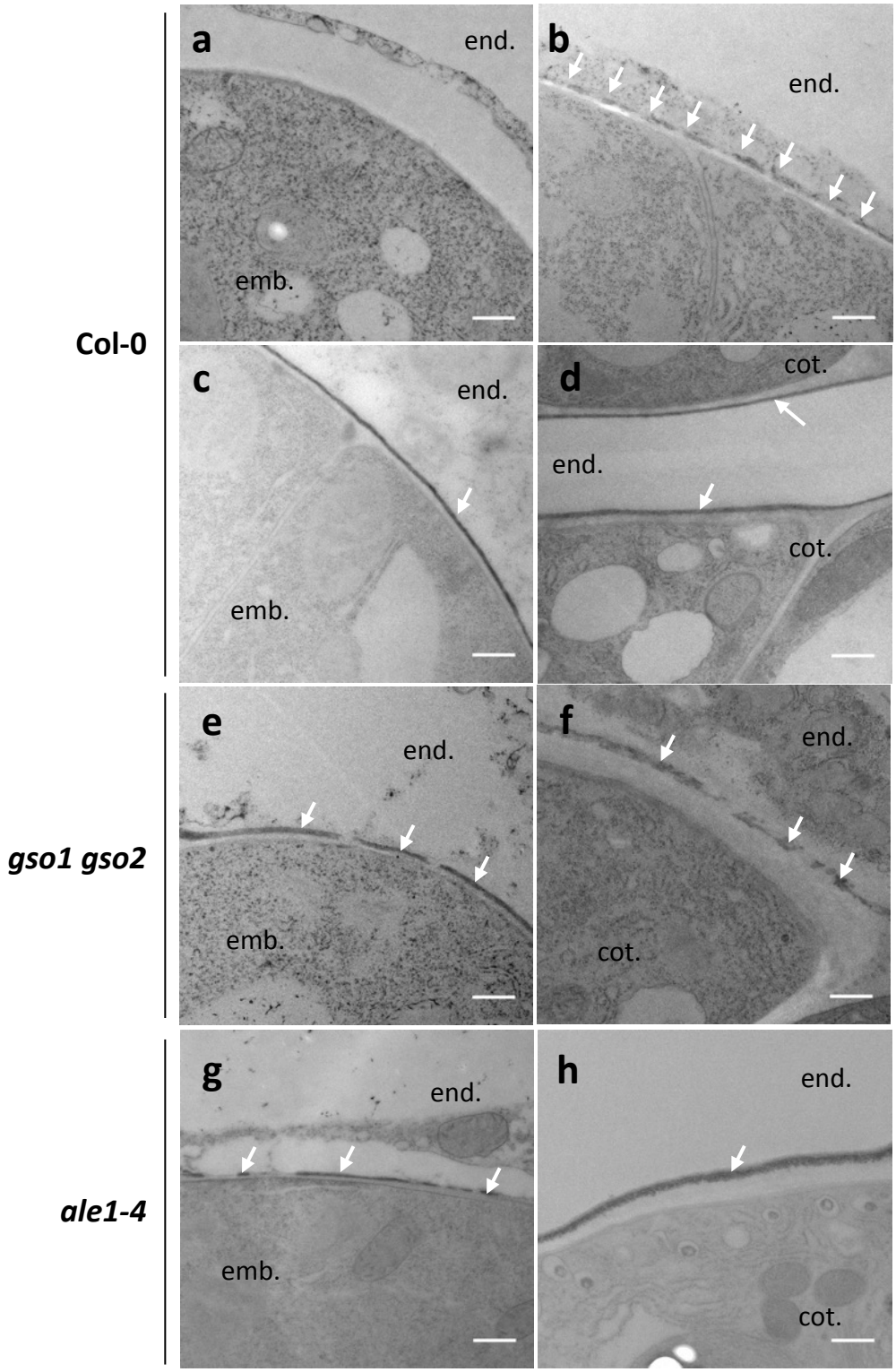

Figure 4

Embryonic cuticle biogenesis involves a process of patch coalescence that is defective in *ale1-4* and *gso1-1 gso2-1* mutants. Analysis of embryonic cuticle deposition in wild-type (a-d), *gso1-1 gso2-1* (e-f) and *ale1-4* (g,h) embryos at 2 cell (a), mid globular (b), mid heart (c,e,g) and walking stick (d,f,h) stages of embryogenesis. White arrows show the external face of the embryonic cuticle. (Embryo (emb.), endospem (end.) and cotyledon (cot.) (for late stages), are labelled. Scale bar = 500nm.

Figure 5

a

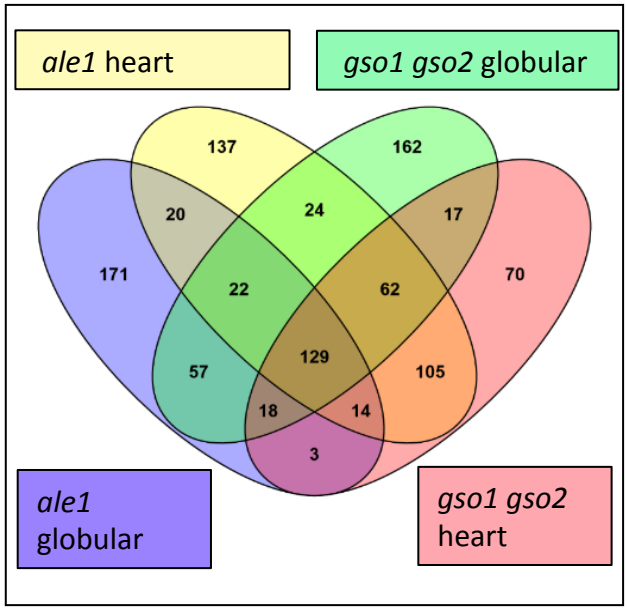

b

Term	p-value
response to chitin	2,58E-26
response to stimulus	3,62E-25
response to carbohydrate stimulus	1,29E-23
response to stress	6,65E-16
response to organic substance	4,69E-15
response to chemical stimulus	7,29E-13
response to wounding	6,71E-11
immune system process	2,42E-10
innate immune response	6,71E-09
immune response	7,81E-09
defense response	9,82E-09
regulation of cellular process	2,31E-08
regulation of biological process	2,36E-08
biological regulation	3,48E-08
regulation of nitrogen compound metabolic process	5,94E-08
regulation of transcription	7,09E-08
response to abiotic stimulus	7,11E-08

Figure 5

ALE1, GSO1 and GSO2 positively regulate the expression of stress-related genes in seeds. (a) Summary of overlaps between gene sets showing reduced expression in *ale1-4* and *gso1-1 gso2-1* mutants at the globular and heart stages of development. (b) GO term analysis of genes down-regulated in both *ale1-4* and *gso1-1 gso2-2* mutants at the heart stage.

Figure 6

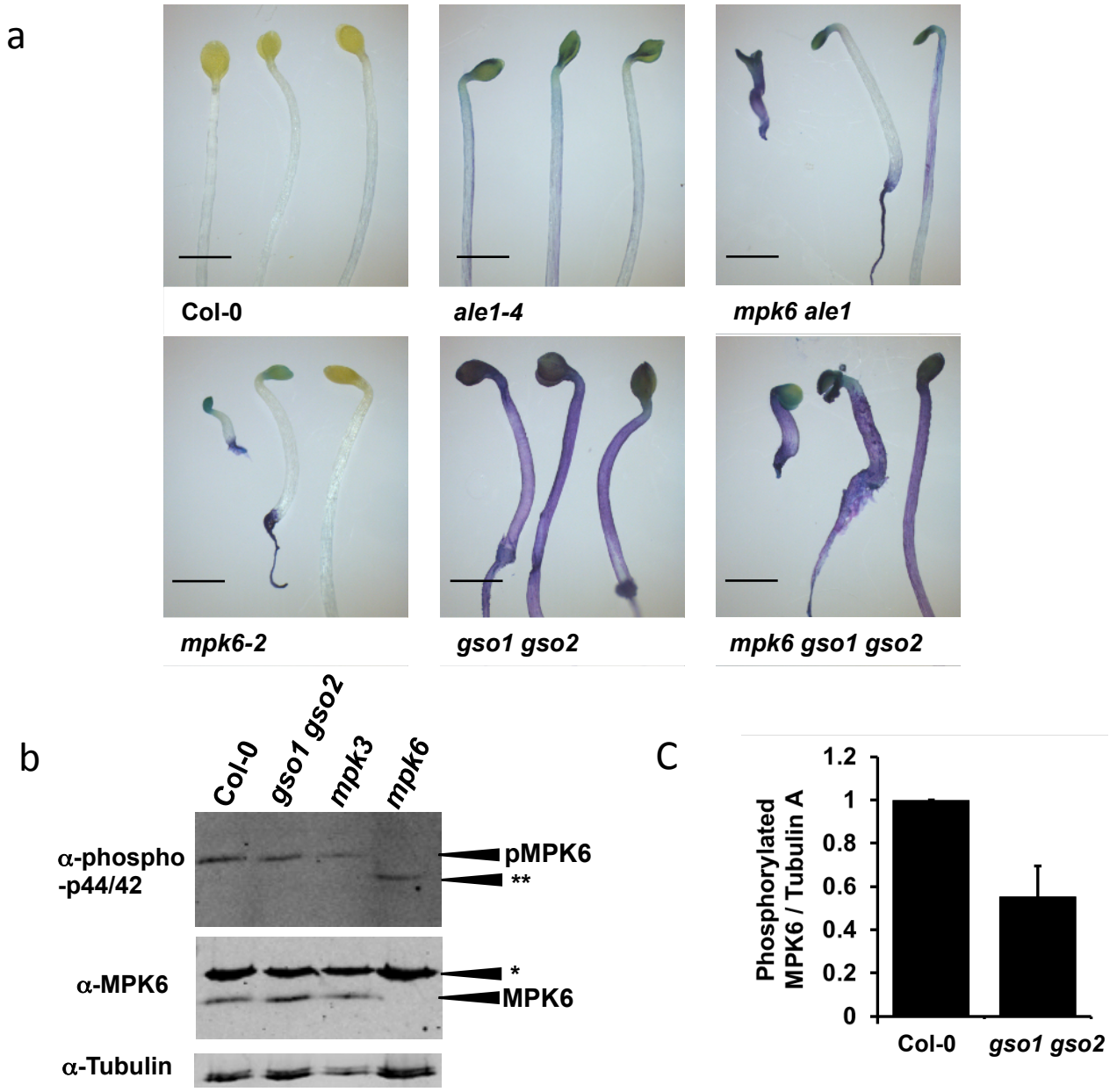

Figure 6

MPK6 acts downstream of ALE1, GSO1 and GSO2 mediated signalling. (a) Seedling cuticle permeability phenotypes of *mpk6-2* and *ale1-4* and *gso1-1 gso2-1* mutants and in double and triple mutant combinations. Scale bar = 2mm (b) Analysis of proteins extracted from developing seeds at the globular-early torpedo stage. The mutants *mpk3-1* and *mpk6-2* were included to confirm band identification. No phosphorylation of MPKs other than MPK6 is observed in Col-0, *gso1-1 gso2-1* or *mpk3-1* seeds, but an additional band (**) is systematically observed in the *mpk6-2* mutant background. * Indicates a non specific band detected by the anti-MPK6 antibody. This experiment was repeated 7 times on independent biological samples, with similar results. (c) Degree of phosphorylation of MPK6 in Col-0 and *gso1-1 gso2-1* mutant seeds. Error bars represent SD of 3 biological replicates (see Supplementary Figure 16 for linearity testing).

Figure 7

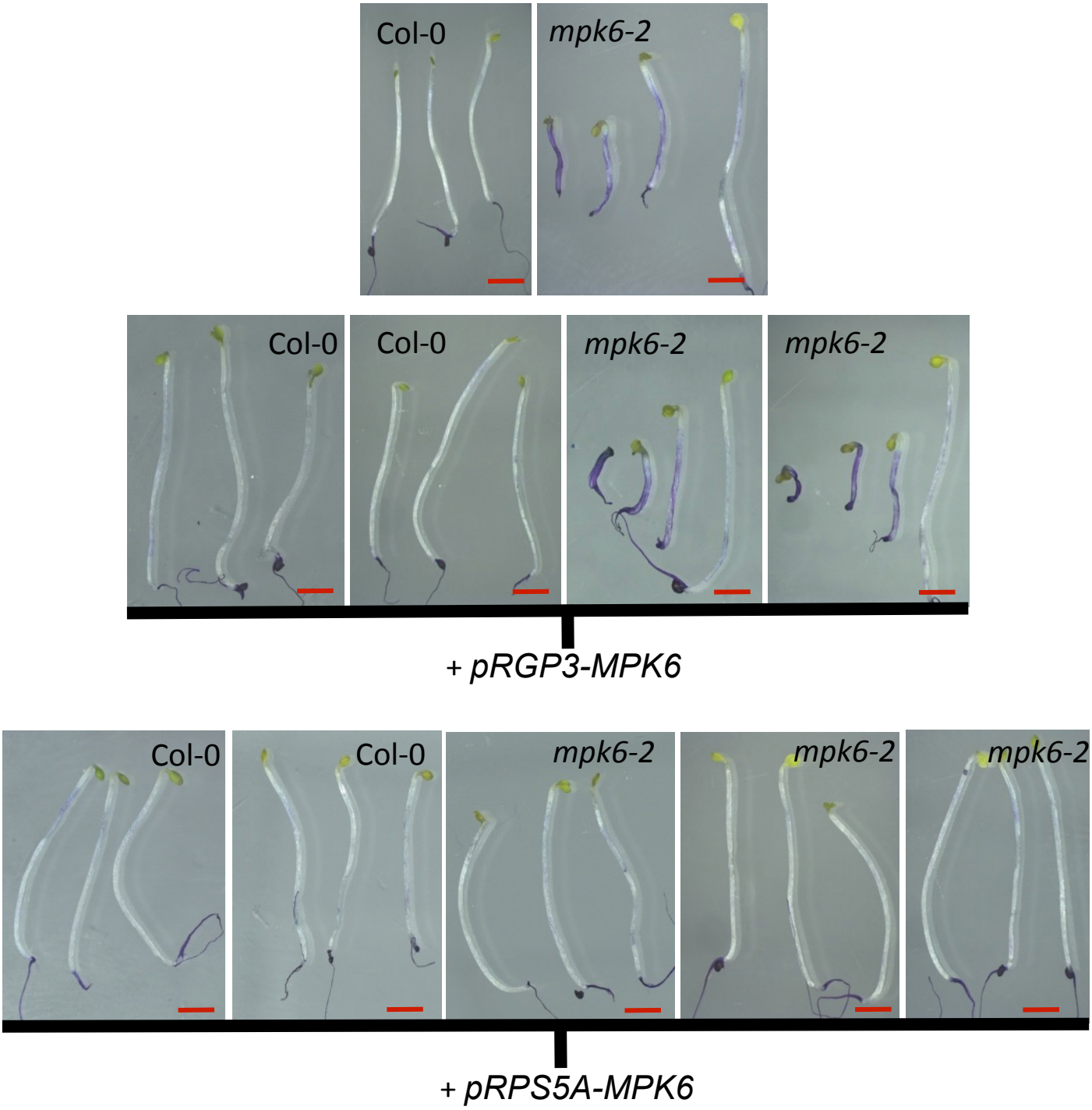

Figure 7.
MPK6 activity is required in the embryo and testa, but not the endosperm, for normal seedling development. (a) Representative phenotypes of toluidine blue-stained seedlings from wild-type (Col-0), *mpk6-2,* and these backgrounds transformed with *pRGP3-MPK6* or *pRPS5A-MPK6.* Lines correspond to those described in Supplementary Figure 17. Scale bar = 2mm